mPD5, an efficacious PICK1 inhibitor for treating chronic pain

Kathrine Louise Jensen[1]*, Nikolaj Riis Chistensen[1,3], Gith Noes-Holt[1], Ida Buur Kanneworff[4], Line Sivertsen[1], Raquel Comaposada Baro[1], Lucía Jiménez-Fernández[1], Carolyn Marie Goddard[1], Chelsea Hopkins[4], Cecilie Dubgaard Thomsen[4], Ahmed Barakat Ibrahim Soltan[4], Marta Díaz del Castillo[4], Sara Elgaard Jager[1], Frederik Grønbæk Tidemand[2], Lise Arleth[2], Anne-Marie Heegaard[4], Andreas Toft Sørensen[1], Kenneth Lindegaard Madsen[1]*

1. *Molecular Neuropharmacology and genetics Laboratory, Department of Neuroscience, Faculty of Health and Medical Sciences, University of Copenhagen, Copenhagen, DK-2200, Denmark.*
2. *X-ray and Neutron Science, Niels Bohr Institute, Faculty of Science, University of Copenhagen, DK-2200, Denmark*
3. *Center for Biopharmaceuticals, Department of Drug Design and Pharmacology, Faculty of Health and Medical Sciences, University of Copenhagen, DK-2100, Denmark*
4. *Department of Drug Design and Pharmacology, Faculty of Health and Medical Sciences, University of Copenhagen, DK-2100, Denmark*

* Corresponding authors:

Kenneth L. Madsen, Molecular Neuropharmacology and genetics Laboratory, Department of Neuroscience, Faculty of Health and Medical Sciences, University of Copenhagen, Copenhagen, DK-2200, Denmark, e-mail: kennethma@sund.ku.dk, phone: +45 23 64 94 01

and

Kathrine Louise Jensen, Molecular Neuropharmacology and genetics Laboratory, Department of Neuroscience, Faculty of Health and Medical Sciences, University of Copenhagen, Copenhagen, DK-2200, Denmark, e-mail: kljensen@sund.ku.dk, phone: +45 26840363.

Number of figures: 6 (+ 3 supplementary figures). Number of tables: 2 (+1 supplementary table)

Acknowledgements: We thank Nabeela Khadim for excellent technical assistance and acknowledge the Core Facility for Integrated Microscopy, Faculty of Health and Medical Sciences, University of Copenhagen. We also thank Fida Biosystems ApS, Denmark for assistance and for allowing us to conduct our experiments at their facilities and we gratefully acknowledge SAXS beam time at the P12 beamline at the PETRAIII at DESY, Germany, along with help from the beamline scientists. This work was supported by a Novo Nordisk Foundation Pre-seed grant (KLM, ATS), Lundbeck Foundation grants R344-2020-1063 (KLM), R322-2019-1816 (KLJ), Independent Research Fund Denmark 2025-00028B (GNH), Innovation Fund Denmark grant 9122-00012B (ATS), and the European Union's Horizon 2020 research and innovation programme under the Marie Sklodowska-Curie grant agreement No 814244 (ABIS, CH).

Author contributions: KLJ, CMG, GNH, and LS were involved in SNI experiments. KLJ performed CFA von Frey experiments and analysis on behavioural data. KLJ and LJF performed CFA anxio-depressive experiments. KLJ performed sePP experiments. IBK, CH, CBT, ABIS and MDC conducted the CIBP experiment and analysed the data with KLJ. NRC and GNH performed and analysed biochemical and biophysical experiments with assistance on SAXS beamtime from FGT and model based SAXS data analysis performed by LA. RCB and LS prepared and stained primary cultures. LS, RCB and SEJ processed and stained tissue. KLM, ATS and AMH supervised the research. KLJ, NRC, KLM, and ATS conceptualized the study, designed the research, and interpreted data. NRC and KLM invented the dimeric peptides. KLJ and KLM wrote the manuscript with contributions from NRC. All authors reviewed and critically evaluated the manuscript.

Conflict of Interest: The lipidated dimeric peptides, their usage, and their extended utilization are disclosed in patent application WO2021/176094 currently being processed by patent authorities. KLM and ATS have ownership interest and are co-founders of Zyneyro, a company having exclusive license rights on the patent, which is owned by the University of Copenhagen, Denmark.

Paper explained

ABSTRACT

Chronic pain is a complex, debilitating and escalating health problem worldwide, impacting one in five adults. Current treatment is compromised by dose-limiting side effects including high abuse liability, loss of ability to function socially and professionally, fatigue, drowsiness, and apathy. PICK1 has emerged as a promising target for the treatment of chronic pain conditions. Here, we develop and characterize a cell-permeable fatty acid conjugated bivalent peptide inhibitor of PICK1 and assess its effects on chronic pain. The myristoylated myr-NPEG$_4$-(HWLKV)$_2$, (mPD5), self-assembles core-shell micelles that provide favourable pharmacodynamic properties and relieves ongoing and evoked mechanical hypersensitivity, thermal hypersensitivity as well as anxio-depressive symptoms in an inflammatory pain model following subcutaneous administration. Further, mPD5 dose-dependently relieves pain in two neuropathic pain models without affecting motor behaviour. Finally, neuropathic pain was relieved far into the chronic phase (18 weeks post SNI surgery) and while the effect of a single injection ceased after a few hours repeated administration provided pain relief lasting up to 20 hrs after last injection.

Keywords: peptide inhibitor, pain treatment, PICK1 peptide inhibitor, lipidated peptide, dimeric peptide, PDZ domain inhibitor, diabetic neuropathy treatment, bone cancer treatment, spontaneous pain treatment, neuropathic pain treatment.

INTRODUCTION

The International Classification of Diseases 11th Revision (ICD-11) defines chronic pain (MG30) as a multifactorial syndrome of pain persisting for more than 3 months with psychological, biological, and social factors contributing to the syndrome (WHO, 2021). Chronic pain involves central plasticity in the spinal cord and supraspinal areas and is characterized by neuropathic as well as inflammatory aspects (Gangadharan *et al*, 2011; Hartmann *et al*, 2004; Nagy *et al*, 2004; Tan & Kuner, 2021; Xu & Yaksh, 2011). Despite complying to recommended treatment guidelines, a large fraction of the 1.5 billion people suffering from chronic pain experience compromised quality of life with constant pain and impairment of work and social life (Goldberg & McGee, 2011; Mills *et al*, 2019). First-line treatments show very low efficacy of chronic pain relief, with numbers to treat (NTTs) ranging from 6 to 10 depending on the aetiology of the pain condition (Finnerup *et al*, 2015; Mills *et al.*, 2019; Reinecke *et al*, 2015), while opioid-based treatments entail a significant risk of high opioid use and addiction (Kaye *et al*, 2017a; Kaye *et al*, 2017b). This highlights an urgent need to develop more effective, non-addictive pain therapeutics.

An emerging strategy for alleviating pain is modulation of receptor trafficking by targeting specific scaffold proteins (Christensen *et al*, 2020; Garry *et al*, 2003; Liu *et al*, 2015). PICK1 (Protein Interacting with C Kinase) is a PDZ domain containing scaffold protein enriched in the postsynaptic density of neurons, known for its role in central synaptic plasticity (Hanley, 2008; Volk *et al*, 2010) and hormone storage and release (Cao *et al*, 2013; Holst *et al*, 2013). PICK1 interacts with a host of membrane proteins and kinases via its PDZ domain (Christensen *et al*, 2019; Erlendsson *et al*, 2014; Madsen *et al*, 2005), many of which have been implicated in pain signalling (Sorensen *et al*, 2022). Notably, PICK1 regulates subcellular localization and surface expression of its interaction partners, including the GluA2 subunit of α-amino-3-hydroxy-5-methyl-4-isoxazolepropionic acid (AMPA) type glutamate receptors (AMPARs) (Hanley, 2008) and acid-sensing ion channels (ASICs) (Hu *et*

al, 2010). PICK1 is expressed in dorsal root ganglions (DRGs) and concentrated in lamina I and the inner lamina II of the dorsal horn (Atianjoh *et al*, 2010; Garry *et al.*, 2003; Wang *et al*, 2011; Wang *et al*, 2016), areas that are all important for the transmission of painful stimuli. Based on studies in animal models using inhibitory peptides, siRNA, and knock-out mice, PICK1 has been shown to be implicated in thermal and mechanical hypersensitivity in neuropathic and inflammatory pain models, advocating PICK1 as a putative target for pharmaceutical intervention of chronic pain states (Atianjoh *et al.*, 2010; Christensen *et al.*, 2020; Garry *et al.*, 2003; Jensen *et al*, 2021; Wang *et al.*, 2011).

Developing small molecule inhibitors of PICK1 has proven difficult (Bach *et al*, 2010; Christensen *et al.*, 2019; Thorsen *et al*, 2010) with some progress in the last decade (Alfonso *et al*, 2014; Lin *et al*, 2018; Marcotte *et al*, 2018). Our recent development of a membrane permeable, bivalent high-affinity PICK1-inhibitor, TPD5 (Christensen *et al.*, 2020), displaying low nanomolar target affinity, represented a major leap towards a potential PICK1 targeting therapeutic. Functionally, TPD5 reduces the interaction between PICK1 and the GluA2-subunit of AMPAR leading to reduced phosphorylation and downregulation of AMPAR surface expression in the spinal cord. Further, intrathecal administration of TPD5 fully alleviated mechanical hypersensitivity in the spared nerve injury (SNI) model of neuropathic pain. No drug tolerance was observed by repeated dosing and equally strong treatment effect was evident beyond the initial phase of the model independent of sex (Christensen *et al.*, 2020). These findings highlight PICK1 as a promising pain target and point to alternative strategies to current treatments and ongoing clinical trials. However, drugs featuring cell-permeable peptides have yet to be approved by FDA or EMA, and concerns have been raised over the safety profile for TAT-conjugated peptides for a drug intended for chronic use in particular (Kilk *et al*, 2009; Waldeck *et al*, 2009) and (TAT NR2B9c, US patent 8,080,518 B2).

In recent years, the use of fatty acid modifications on peptides has emerged as a successful way to enhance both plasma stability and permeability of pharmaceutical peptides while also offering a

benevolent toxicology profile (Knudsen & Lau, 2019; Menacho-Melgar *et al*, 2019; Missirlis *et al*, 2009). Here, we describe the development of a lipid-conjugated variant of this high-affinity bivalent PICK1 inhibitor, myristoylated myr-NPEG$_4$-(HWLKV)$_2$, (mPD5). This molecule demonstrates high stability and solubility due to its intrinsic self-assembly into spherical core-shell micelles with an aggregation number of around 20. It further demonstrates high plasma protein binding as well as satisfactory distribution and elimination properties all compatible with further drug development. Functional characterization of mPD5 following subcutaneous administration in mice shows robust relief of mechanical and thermal hypersensitivity in the Complete Freund's Adjuvant (CFA) model of inflammatory pain. Moreover, in the CFA model, mPD5 reverses anxio-depressive symptoms in the CFA model of inflammatory pain (assessed by marble burying and elevated plus maze tests) and ongoing pain (assessed by single exposure placed preference). In mice, mPD5 also relieves mechanical hypersensitivity in the Spared Nerve Injury (SNI) model of neuropathic pain, and in the STZ model of diabetic neuropathy, but not in a bone cancer pain model (CIBP). mPD5 does not affect basal locomotion of naïve mice in an open field test. Finally, repeated administration of mPD5 gives rise to sustained relief of mechanical hypersensitivity lasting 20 hours after the last administration, advancing the molecule as a strong lead molecule in the clinic for the treatment of chronic pain conditions.

RESULTS

mPD5 oligomerizes into micelle structures

We have previously developed and characterized a peptide inhibitor, TAT-NPEG$_4$-(HWLKV)$_2$ (TPD5), showing promise as a therapeutic lead for the treatment of neuropathic (Christensen *et al.*, 2020) and inflammatory pain (Jensen *et al.*, 2021). High-affinity inhibition of PICK1 was achieved by a bivalent configuration by NPEG$_4$ (P) of the C-terminal five residues of the dopamine transporter (D5). From the same scaffold NPEG$_4$-(HWLKV)$_2$ (PD5) (Figure 1A), we here substituted the TAT cell-penetrating peptide (CPP) sequence with a C_{14} fatty acid (myristoyl acid, myr) to reduce potential side-effects, and to facilitate plasma stability and distribution. This was achieved by direct coupling to the central amide in the NPEG-linker that joins the two PDZ-binding pentapeptides, resulting in the bivalent peptide inhibitor, myr-NPEG$_4$-(HWLKV)$_2$ (mPD5) (Figure 1B). This compound demonstrated excellent stability as we observed no degradation, as determined by mass spectrometry, or change in pH after incubation for 30 days in PBS at either 5 °C or 25 °C (Table 1). Moreover, mPD5 was soluble to at least 250 mg/mL (~130 mM) in PBS as judged from full transparency and monophasic appearance.

We hypothesized that these attractive properties might arise from an oligomeric or core-shell micellar self-assembly of the peptide when brought in aqueous solubilization and with the hydrophobic lipid forming a central core and the mainly hydrophilic PEG$_4$-linked 5-mer peptide facing the aqueous solution. To test this, we used size exclusion chromatography (SEC) (Figure 1C). Indeed, we found that mPD5 self-assembled and eluted at ~14.2 mL, independent of initial concentration, whereas PD5, lacking the myristoyl acid, eluted at ~21 mL (Figure 1C). To investigate this further, we used Small Angle X-ray Scattering (SAXS), which has earlier been used to investigate micelle structures of detergents (Lindner & Zemb, 2002) to reveal if mPD5 self-assemble into micellar structures and to determine the micelle structure and size. The obtained SAXS data (Figure 1D and S1) were indeed

characteristic for core-shell micellar particles. In particular they exhibited a significant oscillation at high-*q*, which would be expected for particles with an inner oscillation of the excess scattering length density that could appear due to a lower density of the hydrocarbon based hydrophobic core of the micelles and a higher density of the surrounding peptide based shell. An extended flat Guinier region was clearly visible at low-*q* values pointing towards rather small micelles without presence of larger aggregates. Further analysis of the low-*q* region showed that the forward scattering (I_0) of mPD5 scaled linearly with concentration (Figure S1A). This suggested that the particle size was concentration independent and that there was no significant interparticle interactions in the studied concentration range (0.3 - 5 mM). The pair-distance distribution, *p(r)*, showed a D_{max} in the range of 50 Å to 55 Å and a shape with a significant shoulder at around 15 Å, a dip at around 20 Å and then a peak at around 30Å (Figure S1C). This shape and its modulation is classic for core-shell particles (Arleth, 1997; Lindner & Zemb, 2002). The values for the radius of gyration, R_g is at around 30 Å but due to the inner structure of the particles the value cannot be interpreted as directly as for homogenous particles, and it was not used in the further analysis.

We next fitted the SAXS data using a molecularly constrained model for spherical core-shell micelles composed by an inner core of the fatty acid part of mPD5 and an outer shell of the peptide part of mPD5 (Figure 1E and S1B and full model account in Materials and Methods). The refined parameters from the fitting suggested that on average ~20 mPD5 molecules make up the assembled micelle, with a hydrophobic core radius of R_{core} = 12.2 Å, a hydrophic shell thickness of D_{shell} = 10.4 Å and hence a total radius, R_{Total} = 22.6 Å) (Figure 1E and supplementary table S1). Since the critical micelle concentration (CMC) of mPD5 is below the detection limit for SAXS and SEC, we used flow-induced dispersion analysis (FIDA) to determine the CMC of mPD5 (Figure 1F). FIDA suggested a CMC of 12 μM (Figure 1D), and a hydrodynamic radius (R_H) of ~ 30 Å (Figure S1C), which is in good

agreement with the SAXS-derived total average radius since the hydrodynamic radius of a spherical particle is often observed to be slightly larger than its geometrical radius.

mPD5 binds PICK1 with high affinity

Using fluorescence polarization competition binding, we determined the affinity ($K_{i,app}$) of mPD5 for PICK1 to be 3.0 nM (SEM interval [2.3-3.8] nM), which is similar to TPD5 ($K_{i,app}$ = 3.9 nM, SEM interval [3.5-4.4] nM), demonstrating a ~1000-fold affinity gain compared to D5 (HWLKV) alone ($K_{i,app}$ = 6.9 µM, SEM interval [5.0-9.9] µM) (Figure 1G). We hypothesize that the self-assembly of mPD5 (Figure 1C-F) is the main driver for the enhanced affinity compared to PD5 ($K_{i,app}$ = 98 nM, data from (Christensen *et al.*, 2020).

To evaluate the ability of micellar mPD5 to bind PICK1, we incubated recombinant full length PICK1 (40 µM) with mPD5 in a concentration corresponding to the CMC (10 µM) and observed a distinct shift in the peak elution volume of PICK1, from 10.9 mL in absence of mPD5 to two peaks at 8 mL and 9 mL in presence of mPD5 (Figure 1H). This constituted a significantly larger shift than what was earlier seen for TPD5 (~1 mL) (Christensen *et al.*, 2020), suggesting the ability of mPD5 to induce a higher order complex than a simpler, bivalent PICK1 inhibitor, such as TPD5 (Christensen *et al.*, 2020).

mPD5 binds to human serum albumin in plasma

Fatty acids are reported to mediate drug binding to serum albumin, thereby enhancing plasma lifetime due to reduced renal clearance and metabolism (Knudsen & Lau, 2019; Menacho-Melgar *et al.*, 2019). Since mPD5 is lipidated and self assembles into micelles, we next assessed if the self-assembly properties were dominant in plasma, or if the fatty acid binding to human serum albumin (HSA) could compete for mPD5 oligomerization in plasma. To this end, we first measured the binding of

fluorescent mPD5 (AF488-mPD5) to HSA through FIDA (Figure 2A-C) and found an affinity of AF488-mPD5 for HSA of 787 nM, which is 15-fold higher than the critical micellar concentration (CMC) (Figure 1F). R_H further suggest that mPD5 binds to dimeric HSA (Figure 2A-C). To evaluate if mPD5 favours self-assembly, or HSA binding in plasma, we incubated AF488-mPD5 in different concentrations of human plasma and obtained R_H's suggesting binding to HSA is favoured over micelle formation in plasma, even in a concentration of mPD5 (21 mM) i.e., 2000-fold above CMC (Figure 2D and S3). Taken together, our data suggest that the lipid chain drives micellar assembly of mPD5 allowing for high solubility and good stability, as well as high affinity PICK1 binding, while once in plasma, mPD5 preferentially binds to serum albumin at the given concentrations.

mPD5 alleviates mechanical hypersensitivity of inflammatory pain, is cell permeable, and distributes to the spinal cord and DRGs following intrathecal injection.

To assess whether the myristoylation rendered mPD5 membrane permeable, we incubated a primary culture of mouse hippocampal neurons with AF488-mPD5 (10 μM) followed by incubation with Cellmask for plasma membrane visualization. Confocal imaging showed strong staining of individual neurons by AF488-mPD5, whereas the supporting glial layer, surprisingly showed little AF488-mPD5 staining (Figure 3A). A profile view of the 3D stack indicated AF488-mPD5 fluorescence extending throughout the cell, with Cellmask confined to the outer regions of the cell, outlining the plasma membrane (Figure 3A). Next, we performed intrathecal (i.t.) injection of AF488-mPD5 (20 μM, 7μl) and assessed the penetration into the spinal cord and dorsal root ganglions (DRGs) of mice (Figure 3B). Indeed, fluorescence was observed in coronal lumbar spinal cord slices from AF488-mPD5-injected animals, with overall increased fluorescence and accumulation in a low number of cells. Compared to the previously investigated TPD5, which tended to accumulate along the edges of the spinal cord, the penetration of mPD5 appeared more uniform, indicating improved penetration of

mPD5 (Christensen *et al.*, 2020). Lumbar dorsal root ganglions (L3-5) DRGs and the lumbar spinal cord (L3-5) also displayed AF488-mPD5, however only with sparse specific fluorescent signal (Figure 3B). Following the distribution of AF488-mPD5, we tested the effect of i.t. mPD5 (20 µM, 7µl) on pain relief of inflammatory pain in male mice using the complete Freund's adjuvant (CFA)-induced model of inflammatory pain (Figure 3C). The experiment was performed as follows: on day 0, the baseline mechanical paw withdrawal threshold (PWT) was established (PWT between 1 and 2 g forces). Then mice were randomly assigned into treatment vs vehicle groups. On day 0, after baseline testing, the mice were injected with CFA. Consistent with previous studies (Aoki *et al*, 2014; Atianjoh *et al.*, 2010), intraplantar injection of CFA into the hind paw led to mechanical hypersensitivity of the ipsilateral paw, with no effect on the contralateral paw; the gram forces of the von Frey filament needed to induce a paw withdrawal of the ipsilateral hind paw was significantly less after CFA-injection compared to baseline ($p < 0.0001$), a behavioural indication of allodynia (Figure 3C). On day 2 after CFA injection, we assessed the effect of mPD5. I.t. injected mPD5 resulted in a significant relief of mechanical hypersensitivity at 1 hr and 5 hrs after administration with no effect 24 hrs after administration. The efficacy and duration of action of mPD5 was very similar to TPD5 by the same route of administration (i.t.) although with a slightly faster onset kinetics (Christensen *et al.*, 2020).

Subcutaneous administration of mPD5 reduces mechanical and thermal hypersensitivity in a mouse model of inflammatory pain.

Next, we tested the effect of subcutaneously administered (s.c.) mPD5 in the CFA model of inflammatory pain (Figure 4). Intraplantar injection of CFA into the hind paw of male mice led to mechanical hypersensitivity of the ipsilateral paw reversed after 11 days, with no effect on the contralateral paw, whereas mice injected with saline instead of CFA (sham), showed no changes in

their pain threshold (Figure 4A). On day 2 after CFA injection, we assessed the effect of a single s.c. administered high dose (50 µmol/kg) mPD5 on mechanically evoked hypersensitivity. In this setup, 50 µmol/kg mPD5 reversed hypersensitivity 1 hr after injection compared to before injection to a PWT level similar to the uninjured contralateral paw and the previous baseline (Figure 4A).

Next, to assess pharmacokinetic properties of mPD5 and to guide dosing, we assessed dose dependence of the plasma exposure of mPD5 following s.c administration using a five-fold descending dose range (50, 10, 2 µmol/kg) (Figure 4B). Plasma levels were assessed after 0.5, 1, 2, 5 and 12 h. For all doses, we observed an initial increase in plasma concentration reaching maximal concentration after 1 hr (1.4 ± 0.1 mg/mL after 2 µmol/kg injection; 6.2 ± 5 mg/mL after 10 µmol/kg injection; 20.2 ± 0.6 mg/mL after 50 µmol/kg injection) followed by a linear elimination phase on the semi-log scale indicating first order kinetics. The maximal dose and area under the curve both scaled linearly with dose, and $T_{1/2}$ showing a tendency to increase with increasing dose (0.50 ±. 0.07 hr after 2 µmol/kg injection; 0.59 ± 0.07 hr after 10 µmol/kg injection; 0.84 ± 0.03 hr after 50 µmol/kg injection). For all concentrations, the distribution volume was approximately 30 mL indicating good distribution to plasma from the site of injection.

Next, we tested dose dependence of mPD5 in the CFA model after s.c. administration using the doses tested for plasma concentrations (2, 10 and 50 µmol/kg) (Figure 4C). All doses tested, revealed significant reversal of the CFA-induced mechanical hypersensitivity 1 hr post administration, and the 50 µmol/kg dose also showed significant reduction of mechanical hypersensitivity at 5 hrs post injection. This indicates that a plasma concentration of approximately 1 mg/mL is sufficient to evoke a significant reduction in mechanical hypersensitivity.

To test the effect of mPD5 on thermally evoked hypersensitivity in the CFA model, we performed a Hargreaves test, settling on the intermediate dose (10 µmol/kg). On day 0, the baseline paw withdrawal latency (PWL) was established (maximum PWL; 21.3 seconds). Following baseline

testing, mice were injected with CFA and randomly assigned into treatment vs vehicle groups. Intraplantar injection of CFA into the hind paw led to thermal hypersensitivity of the ipsilateral paw, a behavioural indication of thermal hyperalgesia, which was reversed by mPD5 (10 µmol/kg) 1 hr after administration. No effect of either CFA or mPD5 was observed on the contralateral paw (Figure 4D).

mPD5 reduces pain related behaviours in a mouse model of inflammatory pain.

In the clinic, several comorbidities of chronic pain have been identified including anxiety, depression and fatigue (Dahan *et al*, 2014). Mechanically and thermally evoked hypersensitivity does not assess aspects of ongoing pain, functional impairment or anxio-depressive symptoms associated with pain, all of which are important aspects of clinically relevant pain (Wilkerson *et al*, 2018). Therefore, we used the combination of a marble burying test, elevated plus maze, and single exposure place preference (sePP) to qualify the therapeutic relevance of mPD5 (Figure 4E-I). In the marble burying test (Figure 4E), CFA injection led to significantly decreased marble burying, presumably anxiogenic, whereas this decrease was reversed significantly by treatment with 10 µmol/kg mPD5 to the level of the naïve mice. In the elevated plus maze test (Figure 4F), CFA injection led to significantly decreased time spent in the open arms, presumably reflecting an anxiogenic effect, whereas CFA animals treated with 10 µmol/kg mPD5 spent an equal amount of time in the open arms as control animals injected with PBS. Finally, we used a single exposure place preference setup (Runegaard *et al*, 2017) to estimate the initial perception of the drug as a measure of relief of ongoing pain (Figure 4G-I). The experiment was performed in a three-compartment apparatus with a striped and a grey compartment separated by a neutral zone (Figure 4G). CFA animals were injected with either PBS in both compartments, or 30 µmol/kg mPD5 in the grey (paired) compartment and PBS in the striped (unpaired) compartment (Figure 4H). Interestingly, the CFA animals treated with mPD5 spent

significantly more time in the paired compartment compared to the PBS animals, indicating a positive effect of mPD5 on spontaneous/ongoing pain. Due to the high abuse liability of the current chronic pain treatments (Smith *et al*, 2016), we repeated the experiment on naive mice to assess putative intrinsic rewarding properties of mPD5 (Figure 4I). The initial sensitivity to the rewarding properties of drugs is believed to be an important endophenotype in relation to the vulnerability to addiction (Lambert *et al*, 2006). Importantly, such control animals did not show any preference for mPD5 compared to PBS (Figure 4I).

mPD5 reduces mechanical hypersensitivity in mice following spared nerve injury and streptozocin injection, but not in cancer-induced bone pain.

We next evaluated the pain-relieving effects of mPD5 in different neuropathic pain models. First, we investigated the effect of mPD5 in the spared nerve injury (SNI) model in male mice (Figure 5A). We found that 10 µmol/kg mPD5 administered s.c. significantly reduced mechanical hypersensitivity up to 3 hrs, whereas a 2 µmol/kg dose showed no significant effect indicating slightly lower potency in the SNI model as compared to the CFA model. Next, we assessed the treatment efficacy of mPD5 to relieve diabetic neuropathy using the streptozocin (STZ) model of type-1 diabetes in male mice (Figure 5B). On day 0, the baseline mechanical PWT was established, followed by injection of STZ. On day 7 after STZ injection, all mice presented a drastic increase of glycemia (from 197.4 +/- 4.4 mg/dL to 533.5 +/- 10.4) validating the diabetic state of the mice. STZ injection led to a significant decrease in PWT on day 13 versus baseline, a behavioural indication of mechanical allodynia (Figure 5B). Since, the STZ model affects both paws equally, we used the established pain-relieving drug pregabalin as a positive control in the experiment instead of the contralateral paw. mPD5 (2 and 10 µmol/kg) administered s.c. resulted in a significant relief of mechanical hypersensitivity at 1 hr post injection, which for the animals injected with the highest dose, lasted another hour. The positive

control (pregabalin) resulted in significant pain relief up to 4 hrs after injection, whereas the vehicle (PBS) had no effect.

Finally, we assessed the effect of mPD5 in a cancer-induced bone pain (CIBP) model (Figure 5C-E). Mice were inoculated with a sarcoma cell line (NCTC 2472) in the femur marrow cavity. Pain-like behaviour was assessed every second day until meeting the criteria of a limb use score of 2 or below in combination with a weight bearing ratio of 0.35 where they received treatment with mPD5 (s.c. 10 μmol/kg) or vehicle. Mice met the criteria at 12-26 days after inoculation. Since symptoms of pain are notoriously challenging to relieve in CIBP models, we used morphine as a positive control. Indeed, morphine (s.c., 5 mg/kg) gave rise to a partial but significant increase in PWT, limb use score and weight bearing ratio in the animals, whereas mPD5 and vehicle had no effect on either.

High doses of mPD5 does not significantly affect basal locomotion in mice.

Finally, we tested if mPD5 affected general locomotion, which could indicate negative side effects of mPD5 (Figure 5F). Mice were injected with 0, 30 or 50 μmol/kg mPD5 s.c. (3- and 5-times higher dose than effective dose administered in CFA and SNI models) and placed in their home cage. After 60 min, which is when the drug is known to have pain-relieving effects, they were placed in a classic open field box and their locomotion monitored for further 60 min (Figure 5F). Although a tendency towards less locomotion was seen for 50 μmol/kg, this effect was not significant (Figure 5F).

mPD5 provides sustained relief of mechanical hypersensitivity in the chronic phase of neuropathic pain.

To test for putative development of tolerance due to down-regulation of the target or other adaptive mechanisms, we carried out a full dose-dependence of mPD5 in the chronic phase of the SNI model (3 weeks after surgery) in mice on two consecutive days (Figure 6A). We observed dose-dependent

relief of the mechanical hypersensitivity for all concentrations tested giving rise to significant effects at 1 hr, while only the 50 µmol/kg showed a significant effect at 5 hrs. Administrations the following day also dose-dependently relieved mechanical hypersensitivity. Only the two highest concentrations showed significant pain relief, but now at both 1 hr and 5 hrs after administration. Taken together this experiment does not indicate immediate development of tolerance.

With this in mind, we sought to obtain sustained relief of mechanical hypersensitivity by consecutive administrations of mPD5. To estimate dose and dosing interval for maintaining a steady state plasma concentration, we employed van Rossum's equation using parameters obtained from the single administration (D = 10 µmol/kg, Vd ~ 30 ml, $T_{1/2}$ = 0.6 hr). This predicted that a steady state plasma concentration of ~2 mg/mL could be maintained by repeated dosing of 2 µmol/kg once an hour following the 10 µmol/kg bolus. We experimentally verified this prediction by assessing the plasma exposure following a single s.c. injection of 10 µmol/kg mPD5 followed by 4 consecutive administrations of 2 µmol/kg with 1 hr intervals (Figure 6B). Blood samples were taken at 5 min, 30 min, 1 hr, 5 hrs, 12 hrs, 24 hrs and 48 hrs after last administration. Notably, the level immediately after the last injection was 2.8 ± 0.5 mg/mL in good agreement with model prediction. The subsequent kinetics was comparable to the single administration with a $T_{1/2}$ of 0.52 ± 0.02 hrs.

Next, we assessed how a repeated administration paradigm giving rise to a steady state plasma level of the drug would affect mechanical hypersensitivity in the SNI model. To this end, we used mice in the very late stage of the model (18 weeks post-surgery) which were injected with either 10 + 2 + 2 + 2 + 2 µmol/kg mPD5 (Group A) or 10 + 0 + 0 + 0 + 2 µmol/kg mPD5 as reference (Group B) (1 hr between injections) (Figure 6C). The consecutive administration not only showed sustained relief of mechanical hypersensitivity but surprisingly also extended the duration of mPD5 to provide significant relief of mechanical hypersensitivity from 1 hr to 25 hrs (20 hrs following last injection). Finally, we asked if such extended duration of action could be obtained by using peptides where the

myristoyl acid was exchanged by longer acyl chains to increase their plasma lifetimes (Nissen *et al*, 2015). For this, we tested peptides conjugated with C18 (stearic acid) and C20 (arachidic acid) fatty acids to produce sPD5 and aPD5, respectively (Figure 6D-F). Single s.c. administration of sPD5 and aPD5 both caused profound itching in the mice, but nonetheless relieved mechanical hypersensitivity in the SNI model similar to mPD5 2 hrs after injection. Similar to mPD5, however, there was no effect on mechanical hypersensitivity 8 hrs after injection suggesting that the extended effect could not be achieved by increasing the length of the fatty acyl chain only.

DISCUSSION

In this study, we have shown that mPD5 relieves pain in 3 different pain models; the CFA model of acute inflammatory pain as well as the SNI and STZ models of chronic neuropathic pain. It is important to note, that these pain models infer very different types of pain. Not only do the models differ in modelling transient versus chronic pain they also differ in being either nociceptive/inflammatory or neuropathic – two very different types of pain entailing fundamentally different aetiologies. Neuropathic pain is initiated or caused by a primary lesion or disease in the somatosensory nervous system, whereas inflammatory pain is the result of nociceptive pain pathways being activated and sensitized by mediators released at sites of tissue inflammation. (Woolf & Salter, 2000; Xu & Yaksh, 2011). In inflammatory models, like the CFA model, pain arises because of tissue damage leading to hyperalgesia in that area, meaning that the pain typically resolves as the tissue heals. In chronic neuropathic pain models, like the SNI model, however, the pain is persisting and does not resolve with healing. Importantly, a number of changes occur in the dorsal root ganglia, as well as the dorsal horn following both types of pain (Xu & Yaksh, 2011). One of these changes is the strengthened synaptic efficacy of the spinal cord dorsal horn, in part developing from an enhanced function of postsynaptic glutamate receptors (Liu *et al.*, 2015; Liu & Salter, 2010; Xu & Yaksh, 2011). Since, mPD5 works on both pain models and is highly efficacious following intrathecal injection, it is likely that mPD5 influences this central sensitization. Importantly, this is in accordance with the role of PICK1 in regulating the trafficking of GluA2 containing AMPARs, crucial for central sensitization and the related maladaptive plasticity (Atianjoh *et al.*, 2010; Garry *et al.*, 2003; Park *et al*, 2009; Sorensen *et al.*, 2022; Wang *et al.*, 2016; Xu & Xia, 2006). It is likely, however, that the effect arising from a s.c. administration in the CFA model in part also relies on a peripheral effect of mPD5 similar to that recently described from TPD5. The mechanistic nature of such a peripheral effect remains to be explored. We note that mPD5 showed no effect on cancer induced bone pain. It

is notoriously challenging to relieve pain in this model (Luger *et al*, 2002), however, given the efficacy in the other models the complete lack of efficacy suggests fundamental mechanistic differences in the way these models modify nociceptive transmission. This is supported by previous studies (Honore *et al*, 2000), where murine models of inflammatory, neuropathic and cancer pain each generated a unique set of neurochemical changes in the spinal cord and sensory neurons.

We recently published on a TAT-conjugated, bivalent, high affinity PICK1 inhibitor (TPD5) displaying good efficacy in the SNI model of neuropathic pain and CFA model of inflammatory pain after intrathecal administration in mice (Christensen *et al.*, 2020; Jensen *et al.*, 2021). Efficacy of TPD5, however, was relatively low following systemic administration (i.p. and s.c.) and increased dosing caused significant discomfort in the mice. Symptoms included itching, respiratory abnormality, and immobility, which has been reported for the TAT-CPP also (TAT NR2B9c, US patent 8,080,518 B2). Of additional concern, TAT has been shown to alter gene expression (both induction and repression of specific genes have been seen) in HeLa cells (Waldeck *et al.*, 2009). In the current paper, to circumvent potential safety issues with CPPs, we developed mPD5, which was obtained by substitution of the TAT CPP tag with a C_{14} fatty acid (myristic acid). Myristoylation of simple peptides to modulate synaptic transmission and plasticity has been used previously to render them cell-permeable (Garry *et al.*, 2003; Nishimune *et al*, 1998; Pastalkova *et al*, 2006). In drug development, lipidation of peptides has been employed to enhance plasma stability due to the interaction between lipids and serum albumin (Bech *et al*, 2018; Curry, 2009; Knudsen & Lau, 2019; Menacho-Melgar *et al.*, 2019). Studies have been made to suggest that lipidation allows the formation of higher order structures (Hoeg-Jensen *et al*, 2005; Hutchinson *et al*, 2019; Kokkoli *et al*, 2006), which in itself makes the molecule more soluble and resilient to degradation. Presumably, mPD5 benefits from all these consequences of the myristoylation, and the compound relies on well-known

chemical principles and well tested building blocks that are considered safe in humans (Baumann *et al*, 2014; Knudsen & Lau, 2019). In our case, the alteration from TPD5 to mPD5 allowed for successful s.c. administration which fully relieves mechanical hypersensitivity in the CFA model of inflammatory pain, the STZ model of diabetic neuropathy as well as the SNI model of neuropathic pain. Subcutaneous administration of peptidic drugs is more advantageous than intravenous or intrathecal administration in terms of improving patient compliance, e.g. due to the suitability for self-administration (Kovalainen *et al*, 2015). Subcutaneous injection is further valued due to the avoidance of hepatic and gastrointestinal degradation. Clinically, subcutaneous injection is the most common route of administration for peptides and is used extensively for both continuous and low-dose drug treatment (Diao & Meibohm, 2013; Kim *et al*, 2017; Kovalainen *et al.*, 2015).

Many drugs used in the treatment of chronic pain show highly problematic side effects e.g., opioids having a high risk of addiction (Gostin *et al*, 2017). To investigate the putative addictive properties of mPD5, we performed a single exposure place-preference experiment, since it is believed that the initial sensitivity to the rewarding properties of a specific drug is a relevant indicator of addictive properties of said drug (Lambert *et al.*, 2006; Runegaard *et al.*, 2017). Our initial assessment of the abuse potential of mPD5 is promising (Figure 4I) since the preference for the mPD5-paired compartment is the same as that for saline. That said, the question of mPD5 abuse liability is not exhausted until the drug has been tested in a full-scale conditioned place preference setup or in self-administration experiments.

It has been hypothesized that one of the explanations for the poor translational value of preclinical data of rodents to humans, is due to assessment of hypersensitivity using von Frey and Hargreaves, which relies on measuring withdrawal reflexes (Ma, 2022). Nociceptive withdrawal reflexes are at

the core of protective pain-related behaviour, and both von Frey and Hargreaves tests measure withdrawal reflex. Thus, it is our belief that such measurements shall never stand alone and explains why we also analysed the perceived pain-relieving effects of the animals indirectly in the sePP, marble burying and elevated plus maze setups. The fact that animals with inflammatory pain prefer the mPD5-paired compartment over vehicle treatment in the sePP test is an indication that the effect of mPD5 is not merely reflex inhibition. Moreover, mPD5 reduced anxio-depressive behaviours associated with pain, suggesting the mechanism indeed taps into the complex pattern of symptoms characterizing chronic pain conditions in patients.

In conclusion, we developed and tested a high-affinity inhibitor (mPD5) for treatment of chronic pain. mPD5 has favourable pharmacokinetic properties (easily soluble and highly stable) and alleviates evoked pain (thermal and mechanic) by different routes of administration (i.t. and s.c.), in inflammatory and neuropathic pain models (CFA, SNI, STZ) of transient and chronic pain. Notably, and important for the translational potential of mPD5, it also reduces anxio-depressive behaviour (MBT, EPM) and induces place preference for the treatment-paired compartment of animals in pain. Taken together, these features advocate that mPD5 represents a compelling drug candidate for further preclinical testing before clinical trials and treatment of chronic pain.

Material and Methods

Peptides.

All peptides were ordered from WuXI AppTec (*Shanghai, China*) or TAG-Copenhagen (*Copenhagen, Denmark*) with >95% purity, validated by MS and UPLC. D5 (DAT-C5, HWLKV), NPD5 ($NPEG_4$-$(HWLKV)_2$, TPD5 (YGRKKRRQRRR-$NPEG_4$-$(HWLKV)_2$), mPD5 (myristyol-$NPEG_4$-$(HWLKV)_2$). 5FAM-TD (5FAM-ahx-YGRKKRRQRRRHWLKV), 5FAM-D5 (5FAM-ahx-HWLKV).

Assessment of solubility and stability of mPD5.

Solubility was determined by visual inspection of samples dissolved in increasing concentration in 10 mM PBS as judged from full transparency and monophasic appearance. Stability was addressed by REDGLEAD for four concentration 2, 20, 50 and 200 µM, by leaving mPD5 in PBS at 5 and 25 ºC for 30 days followed by HPLC-UV-MS.

Protein expression and purification.

Full length rat PICK1 (pET41) was, as described earlier (Madsen *et al.*, 2005), expressed in BL21-DE3-pLysS and grown at 37 ºC, induced at OD_{600}= 0.6 with 1 mM IPTG and grown 16 hrs at 20 ºC. Cultures were harvested and re-suspended in 50 mM Tris, 125 mM NaCl, 2 mM DTT (Sigma), 1% Triton X-100 (Sigma), 20 µg/mL DNAse 1 and ½ a tablet cOmplete protease inhibitor cocktail (Roche) pr. 1 L culture. The resuspended pellets were frozen at -80 ºC for later purification. The lysate was cleared by centrifugation (36,000 x g for 30 min at 4 ºC), and the supernatant was incubated with Glutathione-Sepharose 4B beads (GE Healthcare) for 2 hrs at 4 ºC under gentle rotation and then centrifuged at 4,000 x g for 5 min. The supernatant was removed, and the beads were washed twice in 35 mL 50 mM Tris, 125 mM NaCl, 2 mM DTT and 0.01% Triton-X100. The beads were transferred

to PD-10 Bio-Spin® Chromatography columns (Bio-Rad) and washed with an additional 3 column volumes. Each column was sealed and 0.075 U/µL, Novagen® was added for cleavage O/N at 4 ºC under gentle rotation. PICK1 was eluted on ice and concentration was measured on a NanoDrop 3000.

Fluorescence polarization binding.

The competition binding assay was carried out using a fixed concentration of PICK1 (0.5 µM) and fluorescent tracer (5 nM 5-FAM-TD5 or 20nM 5FAM-D5) incubated with increasing concentrations of unlabelled peptides (D5, TPD5, mPD5) using black half-area Corning non-binding surface 96 well plates (Sigma-Aldrich, Ref. no. 3686). The plates were incubated 20 min on ice and the fluorescence polarization was measured on an Omega POLARstar plate (BMG LABTECH) reader using excitation filter at 485 nm and long pass emission filter at 520 nm. The data was plotted and fitted to a competitive binding One Site fit using GraphPad Prism 8.3.

Size Exclusion Chromatography (SEC).

Recombinant PICK1 (40 µM) was mixed for at least 20 min with mPD5 (10 µM) and run on a Superdex200 Increase 10/300. Similarly, mPD5 and PD5 was dissolved in 50 mM Tris (pH 7.4), 125 mM NaCl, 0.01% Triton X-100, 2mM DTT and run on Superdex200 Increase 10/300 measuring the absorption at 254 nm and 280 nm, due to detector saturation at high mPD5 concentrations, data was plotted for 254 nm.

Flow-induced dispersion analysis (FIDA).

FIDA was carried out using a fluorescently labelled (AF488-NHS) mPD5 analogue, and fluorescence was recorded at 488 nm using AF488-mPD5 (25% labelling efficiency) as a tracer (100 nM), using the standard protocol recommended by the manufacturer, in short, mPD5 and AF488-mPD5 (25%

labelling efficiency) was loaded to the FIDA1 instrument, and peptide sample was injected into the capillary followed by a buffer injection. The diffusion of the peptide could then be observed using 488 nm fluorescence, and the hydrodynamic radius was calculated using the FIDA software 2.0 using a single gaussian distribution fit, at 75% and curve smoothing. Resulting hydrodynamic radius was plotted using GraphPad Prism 8.3.

Small Angle X-ray Scattering (SAXS).

Concentration series of mPD5 ranging from 0.18 mg/mL to 9.37 mg/mL was prepared in buffer containing 50 mM Tris-HCl (pH 7.4) and 125 mM NaCl. Samples were measured at the P12 SAXS Beamline, PetraIII, DESY, Hamburg Germany (Blanchet *et al*, 2015). Initial data processing including radial averaging and conversion of the data into absolute scaled scattering intensity, I(q), as a function of the scattering vector q, where $q= 4\pi \sin(\theta)/\lambda$ (θ = half scattering angle, λ = x-ray wavelength) were done using the standard software, procedures and settings at the beamline (Blanchet *et al.*, 2015). The processed scattering data was merged, buffer subtracted and binned using WillItRebin with a binning factor of 1.02. The modelling of the SAXS data was performed using a molecular constrained core-shell model for polydisperse spherical micelles. In brief, it was assumed that the peptide aggregated into polydisperse spherical micelles. Here, the hydrophobic tails form the core, and these are surrounded by the hydrophilic part (the shell) in a spherical micelle. For the modelling, total scattering lengths of 2.26e-10 cm and 2.96e-11 cm were used for the headgroups and tail, respectively. These were calculated by multiplying the number of electrons in the PD5 headgroup (801 electrons) and the C_{13} alkyl chain (105 electrons) by the scattering length of the electron which is just the classical electron radium of 2.82 fm. For the scattering length density calculations, it was assumed that the molecular volume of the C_{13} alkyl chain, $v_{molec\text{-}hydrophobic}$, was 377 $Å^3$ as estimated from Tanfords empirical formula ($V = 27.4 + 26.9n_C$) where n_C denote the number of carbons. i.e. 13 in

this case (Tanford, 1972). The hydrophilic headgroup, $v_{molec\text{-}hydrophilic}$, was as a first estimate assumed to have a mass density corresponding to that of a soluble protein (i.e. 1.35 g/cm^3), this yielded a molecular volume of 2078 Å^3. This value was then taken as a free parameter in the fits and refined to a molecular volume of ~2010 Å^3 corresponding to a mass density of 1.39 g/cm^3 and with very little variation over the fits to the different sample concentrations. Excess scattering length densities of the core and shell of the micelle were then calculated in relation to the scattering length density of water (9.4e10 1/cm^2). Using this molecular constrained model, the volumes of the core and of the shell were coupled internally through the fitted aggregation number, N_{agg} and the implicit assumption of one PD5 headgroup per one C_{13} alkyl chain. The relative polydispersity, $\sigma_{relative}$ was described by a Gauss function of N_{agg}. The Gauss was truncated at ±3σ. Through the fits this value is refined to $\sigma_{relative}$ values of the aggregation number at ~30% for the highest concentrations to up to 50% at the lowest concentrations. Note, however, that this variation in the particle volume translates to about 10%-15% variation of the particle radius. A full overview of the resulting fit-parameters is provided in table S1. As usual a small surface roughness (typical at the order of 2Å) and a small constant background was also necessary for the model to converge (Pedersen, 2013). A more thorough description of the principle of molecular constrained modelling of simple micelle systems can be found in (Arleth, 1997). The model module "PolydisperseMicelles" from the WillItFit software was used for the fitting (Pedersen, 2013).

Animals.

Unless otherwise specified, wild type male C57BL/6NRj mice (Janvier) at 8 weeks of age at beginning of experiment were used. Animals were allowed at least 7 days of habituation to the animal facility before initiation of experiment. Mice were group-housed in a temperature-controlled room, maintained on a 12/12 hr light/dark cycle (lights on at 6 A.M) with free access to standard rodent

chow and water. Experiments involving animals were performed in accordance with guidelines of the Danish Animal Experimentation Inspectorate (permission number 2016-15-0201-00976, 2021-15-0201-01036, 2020-15-020100439) in a fully AAALAC-accredited facility under the supervision of local animal welfare committee. In all animal experiments, the experimenter was blinded to mice treatment.

Drug administration and dosing for animal experiments.

All compounds were diluted in PBS or saline (depending on control) and administered through different routes i.t. (7 µL/mouse)), i.p. (10 µL/g) or s.c. (10 µL/g)) as indicated. Doses of mPD5 was based on previous studies with TPD5 (Christensen *et al.*, 2020) with a subcutaneous dose-range included in the CFA studies further guiding dose selection for SNI, STZ and CIBP studies. Pregabalin dose was chosen based on previous experience from Phenotype Expertise (Marseilles, France). In the CIBP model, a dose of 5 mg/kg was chosen to avoid hyperactivity, though known to provide only partial pain relief in this model. The test battery of the CIBP model was carried out 45 or 90 min after morphine and mPD5 administration respectively to accomodate the peak efficacy of the drugs.

Immunocytochemistry on hippocampal neurons.

Hippocampal neurons were prepared from C57BL/6 mice (p1-p2) of mixed gender on 12 mm Ø coverslips using 24 well plates. The coverslips were coated o/n at 4 ºC with poly-D-lysine 5 µg/mL (Gibco) followed by incubation with laminin 5 µg/mL (Sigma) for 2 hrs at 37 ºC. A monolayer of rat glial cells was pre-seeded 4 days before the culture, and 24 hrs before, the glial media (DMEM supplemented with 10 % FBS and 0.3 % penicillin/streptomycin (Sigma)) was changed to Neurobasal media supplemented with 1% GlutaMax (Gibco), 0.2 % penicillin/streptomycin, and 2% B-27 (Gibco). To dissociate the hippocampi, mice brains were removed and placed in ice-cold dissection

media: HBSS (Gibco) supplemented with 30 mM glucose, 10 mM HEPES (Gibco) (pH 7.4), 1 mM sodium pyruvate (Gibco), 1 % penicillin/streptomycin (Sigma). The brains were cut in half by a sagittal incision, and the medial section facing up the hippocampi were removed. After isolation, the hippocampi were treated with sterile filtered papain solution (116 mM NaCl, 5.4 mM KCl, 26 mM NaHCO3, 2 mM NAH2PO4, 1 mM MgSO4, EDTA, 25 mM glucose, 1 mM cysteine, 0.5 mM Kyrunate, and Papain 20 U ml−1) at 37 ºC for 30 min, and mechanically disaggregated with two different diameters fire-polished Pasteur pipettes 10 times each, and filtered through a 70 µm cell strainer to remove cell debris. The hippocampal cells were seeded and incubated at 37 ºC with 5 % CO_2. Half of the media was changed every 3-4 days. After 22 days in vitro (DIV22), the primary hippocampal neurons were incubated with 10 µM AF488-mPD5 (25% labelling efficiency) or PBS for 1 hr in conditioned media at 37 ºC and rinsed in PBS before staining fixation (4% PFA) for 10 min on ice and 10 min at room temperature followed by PBS wash. The fixed hippocampal neurons were stained with the plasma membrane dye CellMask Deep Red (dilution 1:100,000 from 5 mg/mL in DMSO) for 10 min at room temperature followed by PBS wash. Coverslips were mounted by using DAPI Fluoromount-G® (SouthernBiotech™). Confocal imaging was performed on a Zeiss LSM 780 laser scanning confocal microscope with a 63x objective.

Immunohistochemistry on DRGs and coronal spinal cord slices.

Mice (8 weeks old, male, C57BL/6N from Janvier) were injected i.t. under isoflurane anaesthesia with 7 µl of 0.9% isotonic saline or 20 µM AF488-mPD5 (25% labelling efficiency). After 1 hr, mice were perfusion fixed with PBS followed by 4% PFA. Spinal cord and DRGs were dissected and kept in 4% PFA overnight followed by storage in 30% sucrose for 2 days and embedding in OCT (TissueTek). Tissues were cut on cryostat (Leica CM3050 S). Coronal slices (30 µm thickness) at the level of injection (L3-5) as well as slices from corresponding DRGs (20 µm thickness) were directly

mounted with DAPI Fluoromount-G® (SouthernBiotech™) and imaged using Axio Scan Z1. Image analysis and visualization was performed using Zen (Zeiss) and Fiji software.

Assessment of plasma levels and biodistribution of mPD5.

The mPD5 plasma exposure was determined by (WUXI, China) and done following s.c. injection of 3 male C57BL/6N (vendor: VTLH) mice (7-9 weeks old, fasted) with each concentration of mPD5 (2, 10 and 50 µmol/kg) in sterile PBS. Blood-samples were taken 30 min, 1 hr, 2 hrs, 5 hrs, 12 hrs following injection. For the repeated administration experiment, the initial s.c. injection of 10 µmol/kg was followed by 4 s.c. administrations of 2 µmol/kg with one hour between injections. Following the last injection, blood samples (0.03 mL from saphenous vein or other suitable site) were collected in EDTA-K2 tubes at 5 min, 30 min, 1 hr, 5 hrs, 12 hrs, 24 hrs and 48 hrs and centrifuged (app 4 °C, 3200 g, 10 min) for collection of plasma. Plasma was transferred to 96 well plates and quick-frozen over dry ice and kept at -60 °C until LC-MS/MS analysis. For LC-MS/MS analysis plasma with 0.25% Triton X100 in 50% MeOH/water (6 µL) was quenched with 160 µL of IS1 (internal standard in MeOH (Labetalol & tolbutamide & Verapamil & dexamethasone & glyburide & Celecoxib 100 ng/mL for each)) and the mixture was vortexed for 10 min at 800 rpm and centrifuged for 15 min at 3220 × g at 4 °C. An aliquot of 65 µL supernatant was transferred to a clean 96-well plate and centrifuged for 5 min at 3220 × g at 4 °C, then the supernatant was directly injected for LC-MS/MS analysis. Plasma half-lives were determined from 3 points in the elimination phase. In a separate experiment biodistribution was assessed (plasma, CSF, spinal cord, whole brain) at 2 hrs after single dose of 10 µmol/kg or 1 hr after last injection in the repeated administration paradigm (10 µmol/kg followed by 4 s.c. administrations of 2 µmol/kg with 1 hr between). At these times plasma level were similar between the two paradigms. Plasma, CSF and tissue samples (kept at 4 °C) were processed and analysed as described above.

Locomotion.

Animals were habituated to the experimental room for a minimum of 60 min before initiation of the experiment. At initiation of experiment, the mice were injected subcutaneously (s.c.) with mPD5 (30 or 50 µmol/kg, pH adjusted to approximately 7 with 5 M NaOH) or 0.9 % saline (B.Braun, Germany) and left in their home cage for 60 min. After precisely 1 hr, the mice were placed in an open field (40 cm x 40 cm x 80 cm) for 60 min. A video camera placed above the open field recorded the animals' behaviour and Ethovision XT 13 (Noldus) was used to track the distance travelled by the animal. The experiment was run in cohort with Figure 2B+C of (Jensen *et al.*, 2021)).

Induction of inflammatory pain (CFA model).

Injury was induced on the right hind paw, whereas the contralateral left hind paw was used as internal control of the animal. The inflammatory pain was induced by injection of 50 µL undiluted Complete Freund's Adjuvant (CFA) (F5881, Sigma) unilaterally into the intraplantar surface of the right hind paw, whereas control mice were injected with the same amount of 0.9 % saline (B. Braun, Germany). All intraplantar injections were performed with and insulin needle (0.3 mL BD Micro-Fine) while the animal was under isoflurane anaesthesia (2%) for maximum 60 seconds. Von Frey was applied up to 11 days after unilateral CFA injection depending on the experiment. (For Figure 3C, the experiment was run in cohort with Figure 1A of (Jensen *et al.*, 2021)).

Induction of neuropathic pain (SNI model).

The initial SNI pain experiment (Figure 5A) was performed by Phenotype Expertise, Marseilles, France – Pain and CNS behaviour CRO under supervision of Stéphane Gaillard, PhD (CEO). Surgery was performed on 8-week-old C57BL/6J male mice (Charles River). The spared nerve injury surgery

was performed on anaesthetized mice with a buprenorphine solution (0.05 mg/kg) injected s.c. 30 min before surgery (10 µL/g). For surgery, mice were anaesthetised with ketamine (100 mg/kg, i.p.) and xylazine (10 mg/kg, i.p.) (volume 10 µL/g) with 100 µL of 1% xylocaine solution infiltrated at the site of the incision. The distal trifurcation of the sciatic nerve was identified, and the tibial and common peroneal branches were ligated with polypropylene nonabsorbable 6-0 sutures (Ethicon) and 1 mm was cut out, leaving the sural branch intact. The wound was closed with sutures, and the animals were allowed to recover and returned to their cages. Two subcutaneous injections of buprenorphine (0.05 mg/kg) were performed with an 8 to 12 hours delay decreasing pain due to the surgery act. 7 days post-surgery, a decrease of threshold response to von Frey filaments of ipsilateral hind-paw was confirmed by von Frey filaments, corresponding to neuropathic pain condition. The mechanical threshold response of the operated mice was measured with calibrated von Frey filaments ("up/down" method) and the 50% threshold (g) was calculated.

The remaining SNI pain experiments were performed in-house using the following procedure. SNI surgery was performed on the left hindleg of the mice under 2% isoflurane anaesthesia. Skin on the lateral surface was incised between hip and knee followed by lengthwise division of the biceps femoris muscle leading to exposure of the three branches of the sciatic nerve. Sural branch was left intact, while the peroneal and tibial branches were ligated with a single surgical knot and axotomized distally of the ligation. Wounds were closed with surgical glue and animal were monitored daily for signs of stress or discomfort, but in all cases recovered uneventfully.

Induction of Diabetic neuropathy (STZ model).

Diabetes was induced by a single i.p. injection of 200 µg/mL streptozocin (STZ) solution (100 µL/10 g, Sigma-Aldrich S0130, batch #WXBB7152V) in male 7-week-old C57BL/6J (Charles River) mice. Glycemia was tested before, and 7 days after injection. All injected mice had blood glucose

concentration >350 mg/dL from day 7 and were used for analgesic testing of the compounds from day 14. One mouse had to be euthanized at 7 days post injection. This experiment was performed by Phenotype Expertise, Marseilles, France - Pain and CNS behaviour CRO under supervision of Stéphane Gaillard, PhD (CEO).

Induction of cancer induced bone pain (CIBP model).

Osteosarcoma cell line NCTC 2472 (American Type Culture Collection, CCL-11TM) were cultured for two weeks prior to surgery in NCTC-135 medium (Sigma-Aldrich, Denmark) supplemented with sodium hydrogen carbonate and 10 % equine serum (Sigma-Aldrich, Denmark). On the day of surgery, cells were washed with PBS and incubated with 3 mL trypsin-EDTA for 5 min followed by centrifugation (2800 rpm, 3 min). Supernatant was removed, and cell pellet resuspended in PBS to obtain a cell density of 10^7 cells/mL.

Two separate cohorts of female C3H/HeNHsd mice (Envigo, Netherlands) of 7-8 weeks, were anaesthetized with 6.25 mg/kg xylazine (Rompun vet, 20 mg/mL, Bayer, KVP Pharma + Veterinär Produkte GmbH, Germany, Batch: KV02BHF) and 43.75 mg/kg ketamine (Ketaminol vet, 100 mg/mL, MSD Animal Health, AN Boxmeer, The Netherlands, Batch: A140A01) and received 1.0-1.2% isoflurane (1000 mg/g isoflurane, Attane vet, ScanVet, Piramal Critical Care Ltd., UK, Batch: G123J18B) during surgery. The mouse was placed on a 37˚C heating pad. Both hind legs were shaved, and a small horizontal incision was made under the knee followed by a vertical incision of approximately 0.5 cm until the patellar tendon was exposed. The patellar tendon was moved to the lateral side exposing the distal epiphysis of the femur. A hole was made in the middle of the distal epiphysis by gently pushing a 30 G needle (0.3x12 mm, 30 Gx1/2”, Luer-Lock, CHIRANA T. Injecta, CH30012) through the bone while rotating. The position of the needle was confirmed by X-ray imaging (IVIS Lumina XR Apparatus, Caliper Life Sciences, Belgium). Following resuspension, 10

μL, corresponding to 10^5 NCTC 2472 cells or PBS (sham mice), was injected in the bone marrow cavity with an insulin syringe (1 mL Luer, BD PlastipakTM, 303172) attached to a 30 G needle and left in the femur for 1 min. Bone wax (Harvard Apparatus, BS4 59-9864) was immediately pushed into the hole with a curette until bleeding stopped. The skin wound was closed with two medical clips (Michel Suture Clips, 7.5x1.75 mm, Angthos, 12040-01). Post-surgical analgesia included s.c. injection of 5 mg/kg carprofen (Carprosan vet, 50 mg/mL mixed 1:25 in sterile ddH2O, Dechra, Le Vet Beheer B.V., Netherlands, Batch: 050520) right after surgery and the following day. Post-surgical care included daily severity scoring for four days, and medical clips removed.

Mechanically evoked pain (von Frey test).

Unless otherwise specified, von Frey occurred as described in the following. Animals were habituated to the experimental room for a minimum of 60 min before initiation of the experiment. Mechanical PWT was determined by von Frey measurements of both hind paws. Von Frey filaments ranging from 0.04 to 2 g (g = gram-forces) (0.04, 0.07, 0.16, 0.4, 0.6, 1.0, 1.4, 2.0) were used for determination of mechanical PWT. Filaments in ascending order were applied to the frontocentral plantar surface of the hind paws. Mice were placed in PVC plastic boxes (11.5 cm x 14 cm) on a wire mesh and allowed minimum 20 min habituation prior of experiment initiation. Each von Frey hair was applied five times with adequate resting periods between each application and number of withdrawals recorded. The withdrawal threshold was determined as the von Frey filament eliciting at least 3 positive trials out of the 5 applications in two consecutive filaments. A positive trial was defined as sudden paw withdrawal, flinching and/or paw licking induced by the filament.

For the CIBP model, two habituation sessions were performed on separated days with mice placed in the von Frey equipment for 1-1.5 hrs in the presence of the experimenter on day one and random von Frey pocking with the 0.6 g filament on day 2. Von Frey monofilaments (North Coast Touch Test,

North Coast Medical, Inc.) with target forces of 0.04g, 0.07g, 0.16g, 0.40g, 0.60g, 1.00g, 1.40g, 2.00g, and 4.00g were used. 50 % PWT was found using the "up-down method" (PWT=$10^{Xf+k\delta}$) starting with the 0.6 g filament. Positive response was defined as; withdrawal, shaking or grooming of paw following a 2-3 second stimulation. In case, of unclear response, stimulus was repeated after 10-15 seconds.

For the STZ model, the mechanical threshold response of the injected mice was measured with calibrated von Frey filaments ("up/down" method) and the 50% threshold (g) was calculated. 13 days post injection, a decrease of threshold response to von Frey filaments of the ipsilateral hind paw was confirmed by von Frey filaments, corresponding to diabetic neuropathy. After injection of test compounds on day 14, mechanical threshold was measured at 1 hr, 2 hrs, 4 hrs and 6 hrs and again on day 15. Compounds were diluted in PBS (vehicle) and administered s.c. at 10 µL/g, in doses as indicated (gabapentin, mPD5). This experiment was performed by Phenotype Expertise, Marseilles, France - Pain and CNS behaviour CRO under supervision of Stéphane Gaillard, PhD (CEO).

Thermally evoked pain (Hargreaves test).

A baseline Hargreaves test was performed on day 0 before inflammatory pain was induced as described in section 2.13. In the Hargreaves test, the mouse was placed in a container on a glass table and left to habituate for at least 15 min. Using the Hargreaves apparatus, a heat beam from beneath was directed towards the hind paws of the mouse and the paw withdrawal time is registered automatically. The cut off was set to maximum 30 seconds to avoid skin injury and the experiment was repeated 5 times for each paw with at least 5 minutes in between measurements. On day -1, 2 and 3, mice were habituated to the Hargreaves equipment by placing them in the boxes for about 30 minutes without directing the beam at them.

Repeated and sustained administration of mPD5 in the SNI model.

For the experiment with repeated administration of mPD5 (Figure 6A), mice underwent surgery leading to partial nerve injury, by cutting the peroneal and tibial nerves, producing hypersensitivity of the remaining sural nerve (SNI) as described in the "**Induction of neuropathic pain (SNI model).**"-section. On day 21 after surgery, hyperalgesia was confirmed by using von Frey filaments to induce mechanically evoked hypersensitivity and measure paw withdrawal threshold of the animals as described in the "**Mechanically-evoked pain (von Frey).**"-section. On the same day, mice were injected s.c. with 2, 10 or 50 µmol/kg mPD5 (10 µL/g) and evoked pain was tested again with the use of von Frey filaments at 1 and 5 hrs after injection. 24 hrs after the first injection, mice were injected s.c. with 2, 10 or 50 µmol/kg mPD5 (10 µL/g) again and evoked pain was tested with the use of von Frey filaments at 1, 5 and 24 hrs after the second injection.

For the first experiment with sustained administration of mPD5 (Figure 6B), the mice underwent a baseline von Frey reading as described in the "**Mechanically-evoked pain (von Frey).**"-section and SNI surgery as described in "**Induction of neuropathic pain (SNI model).**"-section. Approximately 18 weeks (125 days) after SNI surgery, hyperalgesia was confirmed with von Frey. On the same day, mice were injected s.c. with 10 µmol/kg mPD5 and evoked pain was tested again at 1hr after injection. Then, mice were injected s.c. with either 2+2+2 µmol/kg mPD5 (group A) or PBS (group B) once an hour for 3 hrs. At 4,5 hrs after the 10 µmol/kg mPD5 injection paw withdrawal threshold was measured again followed by a s.c. injection of 2 µmol/kg mPD5 in all animals. The PWT was measured again at 6 hrs +7 hrs + 8 hrs + 9 hrs + 10 hrs + 11 hrs + 22 hrs + 23 hrs + 25 hrs + 27 hrs + 49 hrs + 121 hrs after the initial 10 µmol/kg mPD5 injection performed on day 125.

Marble burying test.

Inflammatory pain was induced as described in the "**Induction of inflammatory pain (CFA model**)"-section. On day 3 after CFA injection, marble burying test was performed. Animals were habituated to the experimental room for a minimum of 60 min before initiation of the experiment. Mice were injected with saline, PBS or 10 µmol/kg mPD5 (10 µL/g) and left in their home-cage. At 55 min post injection, the mice were placed in a cage with approximately 5 cm of bedding and left to habituate for 5 min. One hour after injection, the bedding was rearranged to be level again, and 20 marbles were evenly spaced on top of the bedding. Mice were given 20 minutes to bury marbles, after which the mouse was returned to home-cage and number of marbles buried (min 2/3) was counted. Experimenter was blinded to treatment groups. Experiment was run in two different cohorts, by two different experimenters, with 10 months between, and showed the same pattern. n = 12 in each group. The same cohort of mice were used for the elevated plus maze and marble burying test with one day in between tests (elevated plus maze run first).

Elevated plus maze.

Inflammatory pain was induced as described in the "**Induction of inflammatory pain (CFA model**)"-section. Two days later, elevated plus maze was performed. Animals were habituated to the experimental room for a minimum of 60 min before initiation of the experiment. Depending on group, mice were injected with saline, PBS or 10 µmol/kg mPD5 (10 µL/g) and left in their home-cage. One hour later, mice were placed in the elevated plus maze for 5 minutes. Video recordings of the 5 minutes were analysed by EthoVision. Experimenter was blinded to treatment groups. Experiment was run in two different cohorts, by two different experimenters, with 10 months between, and showed the same pattern. n = 12 in each group. The same cohort of mice were used for the elevated plus maze and marble burying test, with one day in between tests (elevated plus maze run first).

Assessment of limb use.

Cancer induced bone pain was induced as described in the "**Induction of cancer induced bone pain (CIBP model)**"-section. For the assessment of limb use, all mice from one cage were placed in an empty transparent plastic box and left for ten minutes to habituate. One mouse at a time was moved by tunnel handling or scooping to an identical plastic box for the limb use test. The gait of the mouse was observed for three minutes and scored by the following system: 4 Normal gait, 3 Insignificant limping, 2 Significant limping and shift in bodyweight towards the healthy limb 1 Significant limping and partial lack of use of ipsilateral leg 0 Total lack of use of ipsilateral leg. A score of 0 was used as a humane endpoint. Urine and faeces were cleaned from the plastic box with a dry paper towel between mice from the same cage, and a new plastic box was used for mice from different cages. The limb use test was video filmed for later evaluation if necessary.

Assessment of static weight bearing.

Cancer induced bone pain was induced as described in the "**Induction of cancer induced bone pain (CIBP model)**"-section and the static weight bearing test was performed using an incapacitance tester (Incapacitance Tester, Version 5.2, Linton). Animals went through 3 equipment habituation sessions before baseline testing. For the weight bearing measurements, the mouse was guided into the tube in the correct diagonal position forcing its hind paws to be located on the two individual sensor plates. The sensor plates measured the applied force by the left and right hind leg respectively. The force was measured for three seconds where the mouse should remain still in the same position. While taking the measurement the tail was lifted gently from the sensor plates to avoid interference. Measurements were done in triplicate, where the mouse was removed and reintroduced into the tube between measurements.

Single exposure place preference.

Initial perception of the drugs was measured by single exposure place preference experiments performed in an elongated three compartment apparatus (67.5 cm x 24 cm) with a biased design of different floor textures and wall pattens and a neutral zone in the middle. We have previously shown that mice of both genders exhibit a strong bias towards the striped compartment, and that a single exposure of psychostimulants in the grey compartment sufficiently changes the preference towards that compartment (Jensen *et al.*, 2021; Runegaard *et al.*, 2017; Runegaard *et al*, 2019). For further details of the setup, we refer to (Runegaard *et al.*, 2017). Experiments lasted 3 days with exposure sessions on days 1 and 2 and a preference test on day 3. On each day, animals were moved from the housing facility to the experimental room and allowed to acclimatize for at least 60 min before initiation of the experiment. mPD5 was paired with the grey compartment, known to be the least preferred compartment (Runegaard *et al.*, 2017; Runegaard *et al.*, 2019). All mice from a cage were tested at the same time, but not all were given the same treatment. Mice were weighed and injected s.c. with PBS or 50 µmol/kg mPD5. For the sePP on CFA-injected mice, the injury was induced as described in "**Induction of inflammatory pain (CFA model)**"-section. sePP was run on day 3-5 after CFA-injection, and von Frey was performed on day 0, 2 and 5 as described in the "**Mechanically-evoked pain (von Frey)**"-section.

Statistical analysis for behavioural experiments.

Unless otherwise stated, all data were analysed using GraphPad Prism 9.4.1. and presented as mean +-SEM with the significance level set to $p < 0.05$. For locomotion and elevated plus maze, Ethovision XT 13 (Noldus) was used to track the distance travelled by each animal. For within group analysis (i.e., von Frey experiments) two-way ANOVA followed by Dunnett's post hoc test was used. For between group analysis of multiple time points (i.e., locomotion experiments) two-way ANOVA was

used without post hoc test due to lack of treatment significance in the ANOVA test. For the limb use experiment, data pre versus post treatment was analysed with a Kruskal Wallis test due to the non-parametric nature of the data. When analysing histograms of three groups or more (i.e., marble burying and elevated plus maze) one-way ANOVA followed by Tukey post hoc test was used. When analysing histograms of two groups (i.e. single exposure place preference) unpaired t-test was performed. ROUTS outlier analysis was used for the elevated plus maze identifying 2 outliers, that were removed from the data analysis. The experimenter was blinded to treatment throughout all experiments.

Table of statistics

Figure	Test	Sample size	Statistical data
1A-H	NA	NA	NA
2A-D	NA	NA	NA
3A-B	NA	NA	NA
3C i.t. mPD5 administration in CFA-mice followed by von Frey	Two-way ANOVA followed by Dunnetts *post-hoc* test of time 0 hrs versus 1, 5, 24 hrs	$n_{vehicle} = 5$ $n_{mPD5} = 6$	<u>mPD5:</u> $p_{1hr} = 0.0019$ $p_{5hrs} = 0.0296$ $p_{24hrs} > 0.9999$ <u>Vehicle:</u> $p_{1hr} = 0.9969$ $p_{5hrs} > 0.9999$ $p_{24hrs} > 0.9999$
4A s.c. mPD5 administration in CFA-mice followed by von Frey	Two-way ANOVA followed by Dunnetts *post-hoc* test of time 0 hrs versus 1, 5, 24 hrs	$n_{saline_saline} = 4$ $n_{CFA_saline} = 5$ $n_{CFA_mPD5} = 6$	<u>saline_saline:</u> $p_{1hr} = 0.4778$ $p_{5hrs} > 0.9999$ $p_{24hrs} = 0.9273$ <u>CFA_saline:</u> $p_{1hr} = 0.9988$ $p_{5hrs} > 0.9999$ $p_{24hrs} = 0.9997$ <u>CFA_mPD5:</u> $p_{1hr} < 0.0001$ $p_{5hrs} = 0.5171$ $p_{24hrs} = 0.9985$
4B	NA	NA	NA
4C s.c. mPD5 (2, 10 or 50 µmol/kg)	Two-way ANOVA followed by	$n_{50\ \mu mol/kg} = 5$ $n_{10\ \mu mol/kg} = 6$	<u>2 µmol/kg:</u> $p_{1hr} = 0.0476$

administration in CFA-mice followed by von Frey	Dunnetts *post-hoc* test of time 0 hrs versus 1, 5, 24 hrs	$n_{2\ \mu mol/kg}$ =5	p_{5hrs} = 0.9773 p_{24hrs} = 0.9773 <u>10 µmol/kg:</u> p_{1hr} = 0.0426 p_{5hrs} = 0.1585 p_{24hrs} = 0.9998 <u>50 µmol/kg:</u> p_{1hr} = 0.0001 p_{5hrs} = 0.0345 p_{24hrs} = 0.9690
4D s.c. mPD5 administration in CFA-mice followed by Hargreaves test	Two-way ANOVA followed by Dunnetts *post-hoc* test of time 0 hrs versus 1, 5, 21 hrs	n = 6 in both groups	<u>mPD5:</u> p_{1hr} = 0.0001 p_{5hrs} = 0.3282 p_{21hrs} = 0.9620 <u>PBS:</u> p_{1hr} = 0.8295 p_{5hrs} = 0.8130 p_{21hrs} >0.9999
4E s.c. mPD5 administration in CFA-mice followed by marble burying test	one-way ANOVA with Tukey multiple comparison	n = 12 in each group	<u>CFA:</u> p = 0.0024 <u>mPD5:</u> p = 0.6802 PBS: p = 0.0209
4F s.c. mPD5 administration in CFA-mice followed by elevated plus maze	one-way ANOVA with Tukey multiple comparison	n = 12 in each group	<u>CFA:</u> p = 0.0299 <u>mPD5:</u> p = 0.6903
4G	NA	NA	NA
4H s.c. mPD5 administration in CFA-mice followed by sePP	Unpaired t test	n_{PBS}= 15 n_{mPD5} = 12	<u>mPD5vsPBS:</u> p = 0.0403
4I s.c. mPD5 administration in control mice followed by sePP	Unpaired t test	n = 7 in both groups	<u>mPD5vsPBS:</u> p = 0.9884
5A s.c. mPD5 administration in SNI-mice followed by von Frey	Two-way ANOVA followed by Dunnetts *post-hoc* analysis	n = 6 in each group	<u>PBS:</u> p_{1hr} = 0.8530 p_{2hrs} = 0.9108 p_{3hrs} = 0.9054 p_{4hrs} = 0.7305 p_{6hrs} = 0.6840 <u>2 µmol/kg:</u> p_{1hr} = 0.0633 p_{2hrs} = 0.4194 p_{3hrs} = 0.9423 p_{4hrs} = 0.9998

			$p_{6hrs} = 0.9997$ <u>10 µmol/kg:</u> $p_{1hr} < 0.0001$ $p_{2hrs} < 0.0001$ $p_{3hrs} < 0.0001$ $p_{4hrs} = 0.0668$ $p_{6hrs} = 0.9565$
5B i.p. mPD5 administration in STz-mice followed by von Frey	Two-way ANOVA followed by Dunnetts *post-hoc* test of time 0 hrs versus 1, 2, 4, 6 and 24 hrs	$n_{pregabalin} = 10$ $n_{mPD5} = 10$ $n_{PBS} = 9$	<u>Pregabalin:</u> $p_{1hr} = 0.0046$ $p_{2hrs} < 0.0001$ $p_{4hrs} = 0.0046$ $p_{6hrs} > 0.9999$ <u>Vehicle:</u> $p_{1hr} > 0.9999$ $p_{2hrs} = 0.9961$ $p_{4hrs} = 0.9961$ $p_{6hrs} = 0.9998$ <u>$mPD5_{2\mu mol/kg}$:</u> $p_{1hr} = 0.0186$ $p_{2hrs} = 0.2315$ $p_{4hrs} = 0.2315$ $p_{6hrs} = 0.9998$ <u>$mPD5_{10\mu mol/kg}$:</u> $p_{1hr} < 0.0001$ $p_{2hrs} < 0.0001$ $p_{4hrs} = 0.0894$ $p_{6hrs} = 0.9998$
5C s.c. mPD5 administration in CIBP mice followed by von Frey	Two-way ANOVA followed by Dunnetts *post-hoc* test of pre versus post + baselines	$n_{morphine} = 10$ $n_{mPD5} = 11$ $n_{PBS} = 11$	$p_{pre\text{-}postmPD5} = 0.6484$ $p_{pre\text{-}postmorphine} < 0.0001$ $p_{pre\text{-}postPBS} = 0.7914$
5D s.c. mPD5 administration in CIBP mice followed by limb use test	Wilcoxon matched-pairs signed rank test (non-parametric data)	$n_{morphine} = 10$ $n_{mPD5} = 11$ $n_{PBS} = 11$	$p_{pre\text{-}postmPD5} = 0.5000$ $p_{pre\text{-}postmorphine} = 0.0156$ $p_{pre\text{-}postPBS} = 0.6875$
5E s.c. mPD5 administration in CIBP mice followed by weight bearing test	Two-way ANOVA followed by Dunnetts *post-hoc* test of pre versus post and baselines	$n_{morphine} = 10$ $n_{mPD5} = 11$ $n_{PBS} = 11$	$p_{mPD5} = 0.9995$ $p_{morphine} = 0.0420$ $p_{PBS} = 0.0748$
5F s.c. mPD5 (0, 30 or 50 µmol/kg) administration in control mice followed by open field test	Two-way ANOVA followed by Dunnetts *post-hoc* analysis	$n_{saline} = 7$ $n_{30} = 6$ $n_{50} = 7$	$F_{(2,17)} = 1.124$ $p = 0.3479$

6A repeated s.c. mPD5 administration in SNI mice followed by von Frey	Two-way ANOVA followed by Dunnetts *post-hoc* analysis compared to baseline post SNI	n = 8 in each group	<u>$mPD5_{2\mu mol/kg}$:</u> day 1 $p_{1hr} = 0.0105$ $p_{5hrs} = 0.1037$ $p_{23hrs} = 0.6065$ day 2 $p_{1hr} = 0.0681$ $p_{5hrs} = 0.2325$ $p_{24hrs} = 0.9996$ <u>$mPD5_{10\mu mol/kg}$:</u> day 1 $p_{1hr} = 0.0077$ $p_{5hrs} = 0.2249$ $p_{23hrs} = 0.9794$ day 2 $p_{1hr} = 0.0082$ $p_{5hrs} = 0.0241$ $p_{24hrs} = 0.9997$ <u>$mPD5_{50\mu mol/kg}$:</u> day 1 $p_{1hr} = 0.0026$ $p_{5hrs} = 0.0368$ $p_{23hrs} = 0.9806$ day 2 $p_{1hr} = 0.0008$ $p_{5hrs} = 0.0112$ $p_{24hrs} = 0.7490$
6B	NA	NA	<u>NA</u>
6C sustained s.c. mPD5 administration in SNI mice followed by von Frey	Two-way ANOVA with Dunnetts multiple comparison vs baseline before treatment	n = 8 in each group	<u>Group A:</u> $hour_{1-10}$ $p < 0.0001$ $hour_{11}$ $p = 0.0011$ $hour_{22}$ $p = 0.0121$ $hour_{23}$ $p = 0.1169$ $hour_{25}$ $p = 0.0023$ $hour_{27}$ $p = 0.1125$ $hour_{49}$ $p = 0.1331$ $hour_{121}$ $p = 0.9957$ <u>Group B:</u> $hour_{1}$ $p < 0.0001$ $hour_{4.5}$ $p = 0.1927$ $hour_{6}$ $p = 0.0775$ $hour_{7}$ $p = 0.1063$ $hour_{8}$ $p = 0.7768$ $hour_{9}$ $p = 0.8516$ $hour_{10}$ $p = 0.9997$ $hour_{11}$ $p > 0.9999$ $hour_{22}$ $p = 0.9994$ $hour_{23}$ $p > 0.9999$

			$hour_{25}$ $p = 0.9997$ $hour_{27}$ $p > 0.9999$ $hour_{49}$ $p = 0.9996$ $hour_{121}$ $p = 0.9999$
6D	NA	NA	NA
6E	NA	NA	NA
6F s.c. saline/mPD5/aPD5/sPD5 administration in SNI mice followed by von Frey	Two-way ANOVA followed by Dunnetts *post-hoc* analysis	n = 6 in each group	vehicle: $p_{2hr} = 0.7257$ $p_{8hrs} = 0.6137$ $p_{13hrs} = 0.4137$ mPD5: $p_{2hr} < 0.0001$ $p_{8hrs} = 0.8933$ $p_{13hrs} > 0.9999$ sPD5: $p_{2hr} = 0.0365$ $p_{8hrs} = 0.9501$ $p_{13hrs} = 0.9472$ aPD5: $p_{2hr} = 0.0058$ $p_{8hrs} = 0.4245$ $p_{13hrs} = 0.1971$

REFERENCES

Alfonso S, Kessels HW, Banos CC, Chan TR, Lin ET, Kumaravel G, Scannevin RH, Rhodes KJ, Huganir R, Guckian KM *et al* (2014) Synapto-depressive effects of amyloid beta require PICK1. *Eur J Neurosci* 39: 1225-1233

Aoki Y, Mizoguchi H, Watanabe C, Takeda K, Sakurada T, Sakurada S (2014) Potential involvement of mu-opioid receptor dysregulation on the reduced antinociception of morphine in the inflammatory pain state in mice. *J Pharmacol Sci* 124: 258-266

Arleth LP, D.; Gazeau, D.; Larpent, C.; Zemb, T.; Mortensen, K.; Pedersen, J.S. (1997) Small-Angle Scattering Study of TAC8: A Surfactant with Cation Complexing Potential. *Langmuir* 13: 1887-1896

Atianjoh FE, Yaster M, Zhao X, Takamiya K, Xia J, Gauda EB, Huganir RL, Tao YX (2010) Spinal cord protein interacting with C kinase 1 is required for the maintenance of complete Freund's adjuvant-induced inflammatory pain but not for incision-induced post-operative pain. *Pain* 151: 226-234

Bach A, Stuhr-Hansen N, Thorsen TS, Bork N, Moreira IS, Frydenvang K, Padrah S, Christensen SB, Madsen KL, Weinstein H *et al* (2010) Structure-activity relationships of a small-molecule inhibitor of the PDZ domain of PICK1. *Org Biomol Chem* 8: 4281-4288

Baumann A, Tuerck D, Prabhu S, Dickmann L, Sims J (2014) Pharmacokinetics, metabolism and distribution of PEGs and PEGylated proteins: quo vadis? *Drug Discov Today* 19: 1623-1631

Bech EM, Pedersen SL, Jensen KJ (2018) Chemical Strategies for Half-Life Extension of Biopharmaceuticals: Lipidation and Its Alternatives. *ACS Med Chem Lett* 9: 577-580

Blanchet CE, Spilotros A, Schwemmer F, Graewert MA, Kikhney A, Jeffries CM, Franke D, Mark D, Zengerle R, Cipriani F *et al* (2015) Versatile sample environments and automation for biological solution X-ray scattering experiments at the P12 beamline (PETRA III, DESY). *J Appl Crystallogr* 48: 431-443

Cao M, Mao Z, Kam C, Xiao N, Cao X, Shen C, Cheng KK, Xu A, Lee KM, Jiang L *et al* (2013) PICK1 and ICA69 control insulin granule trafficking and their deficiencies lead to impaired glucose tolerance. *PLoS biology* 11: e1001541

Christensen NR, Čalyševa J, Fernandes EFA, Lüchow S, Clemmensen LS, Haugaard-Kedström LM, Strømgaard K (2019) PDZ Domains as Drug Targets. *Advanced Therapeutics* 2: 1800143

Christensen NR, De Luca M, Lever MB, Richner M, Hansen AB, Noes-Holt G, Jensen KL, Rathje M, Jensen DB, Erlendsson S *et al* (2020) A high-affinity, bivalent PDZ domain inhibitor complexes PICK1 to alleviate neuropathic pain. *EMBO Mol Med* 12: e11248

Curry S (2009) Lessons from the crystallographic analysis of small molecule binding to human serum albumin. *Drug Metab Pharmacokinet* 24: 342-357

Dahan A, van Velzen M, Niesters M (2014) Comorbidities and the complexities of chronic pain. *Anesthesiology* 121: 675-677

Diao L, Meibohm B (2013) Pharmacokinetics and pharmacokinetic-pharmacodynamic correlations of therapeutic peptides. *Clin Pharmacokinet* 52: 855-868

Erlendsson S, Rathje M, Heidarsson PO, Poulsen FM, Madsen KL, Teilum K, Gether U (2014) Protein interacting with C-kinase 1 (PICK1) binding promiscuity relies on unconventional PSD-95/discs-large/ZO-1 homology (PDZ) binding modes for nonclass II PDZ ligands. *The Journal of biological chemistry* 289: 25327-25340

Finnerup NB, Attal N, Haroutounian S, McNicol E, Baron R, Dworkin RH, Gilron I, Haanpaa M, Hansson P, Jensen TS *et al* (2015) Pharmacotherapy for neuropathic pain in adults: a systematic review and meta-analysis. *Lancet Neurol* 14: 162-173

Gangadharan V, Wang R, Ulzhofer B, Luo C, Bardoni R, Bali KK, Agarwal N, Tegeder I, Hildebrandt U, Nagy GG *et al* (2011) Peripheral calcium-permeable AMPA receptors regulate chronic inflammatory pain in mice. *J Clin Invest* 121: 1608-1623

Garry EM, Moss A, Rosie R, Delaney A, Mitchell R, Fleetwood-Walker SM (2003) Specific involvement in neuropathic pain of AMPA receptors and adapter proteins for the GluR2 subunit. *Mol Cell Neurosci* 24: 10-22

Goldberg DS, McGee SJ (2011) Pain as a global public health priority. *BMC Public Health* 11: 770

Gostin LO, Hodge JG, Jr., Noe SA (2017) Reframing the Opioid Epidemic as a National Emergency. *JAMA* 318: 1539-1540

Hanley JG (2008) PICK1: a multi-talented modulator of AMPA receptor trafficking. *Pharmacol Ther* 118: 152-160

Hartmann B, Ahmadi S, Heppenstall PA, Lewin GR, Schott C, Borchardt T, Seeburg PH, Zeilhofer HU, Sprengel R, Kuner R (2004) The AMPA receptor subunits GluR-A and GluR-B reciprocally modulate spinal synaptic plasticity and inflammatory pain. *Neuron* 44: 637-650

Hoeg-Jensen T, Havelund S, Nielsen PK, Markussen J (2005) Reversible insulin self-assembly under carbohydrate control. *J Am Chem Soc* 127: 6158-6159

Holst B, Madsen KL, Jansen AM, Jin C, Rickhag M, Lund VK, Jensen M, Bhatia V, Sorensen G, Madsen AN *et al* (2013) PICK1 deficiency impairs secretory vesicle biogenesis and leads to growth retardation and decreased glucose tolerance. *PLoS biology* 11: e1001542

Honore P, Rogers SD, Schwei MJ, Salak-Johnson JL, Luger NM, Sabino MC, Clohisy DR, Mantyh PW (2000) Murine models of inflammatory, neuropathic and cancer pain each generates a unique set of neurochemical changes in the spinal cord and sensory neurons. *Neuroscience* 98: 585-598

Hu ZL, Huang C, Fu H, Jin Y, Wu WN, Xiong QJ, Xie N, Long LH, Chen JG, Wang F (2010) Disruption of PICK1 attenuates the function of ASICs and PKC regulation of ASICs. *Am J Physiol Cell Physiol* 299: C1355-1362

Hutchinson JA, Hamley IW, Torras J, Aleman C, Seitsonen J, Ruokolainen J (2019) Self-Assembly of Lipopeptides Containing Short Peptide Fragments Derived from the Gastrointestinal Hormone PYY3-36: From Micelles to Amyloid Fibrils. *J Phys Chem B* 123: 614-621

Jensen KL, Noes-Holt G, Sorensen AT, Madsen KL (2021) A Novel Peripheral Action of PICK1 Inhibition in Inflammatory Pain. *Front Cell Neurosci* 15: 750902

Kaye AD, Jones MR, Kaye AM, Ripoll JG, Galan V, Beakley BD, Calixto F, Bolden JL, Urman RD, Manchikanti L (2017a) Prescription Opioid Abuse in Chronic Pain: An Updated Review of Opioid Abuse Predictors and Strategies to Curb Opioid Abuse: Part 1. *Pain Physician* 20: S93-S109

Kaye AD, Jones MR, Kaye AM, Ripoll JG, Jones DE, Galan V, Beakley BD, Calixto F, Bolden JL, Urman RD *et al* (2017b) Prescription Opioid Abuse in Chronic Pain: An Updated Review of Opioid Abuse Predictors and Strategies to Curb Opioid Abuse (Part 2). *Pain Physician* 20: S111-S133

Kilk K, Mahlapuu R, Soomets U, Langel U (2009) Analysis of in vitro toxicity of five cell-penetrating peptides by metabolic profiling. *Toxicology* 265: 87-95

Kim H, Park H, Lee SJ (2017) Effective method for drug injection into subcutaneous tissue. *Sci Rep* 7: 9613

Knudsen LB, Lau J (2019) The Discovery and Development of Liraglutide and Semaglutide. *Front Endocrinol (Lausanne)* 10: 155

Kokkoli E, Mardilovich A, Wedekind A, Rexeisen EL, Garg A, Craig JA (2006) Self-assembly and applications of biomimetic and bioactive peptide-amphiphiles. *Soft Matter* 2: 1015-1024

Kovalainen M, Monkare J, Riikonen J, Pesonen U, Vlasova M, Salonen J, Lehto VP, Jarvinen K, Herzig KH (2015) Novel delivery systems for improving the clinical use of peptides. *Pharmacol Rev* 67: 541-561

Lambert NM, McLeod M, Schenk S (2006) Subjective responses to initial experience with cocaine: an exploration of the incentive-sensitization theory of drug abuse. *Addiction* 101: 713-725

Lin EYS, Silvian LF, Marcotte DJ, Banos CC, Jow F, Chan TR, Arduini RM, Qian F, Baker DP, Bergeron C *et al* (2018) Potent PDZ-Domain PICK1 Inhibitors that Modulate Amyloid Beta-Mediated Synaptic Dysfunction. *Sci Rep* 8: 13438

Lindner P, Zemb T (2002) *Neutrons, X-rays, and light : scattering methods applied to soft condensed matter*. Elsevier, Amsterdam ; Boston

Liu TY, Cheng Y, Qin XY, Yu LC (2015) Pharmacologically inhibiting GluR2 internalization alleviates neuropathic pain. *Neurosci Bull* 31: 611-616

Liu XJ, Salter MW (2010) Glutamate receptor phosphorylation and trafficking in pain plasticity in spinal cord dorsal horn. *Eur J Neurosci* 32: 278-289

Luger NM, Sabino MAC, Schwei MJ, Mach DB, Pomonis JD, Keyser CP, Rathbun M, Clohisy DR, Honore P, Yaksh TL *et al* (2002) Efficacy of systemic morphine suggests a fundamental difference in the mechanisms that generate bone cancer vs inflammatory pain. *Pain* 99: 397-406

Ma Q (2022) A functional subdivision within the somatosensory system and its implications for pain research. *Neuron* 110: 749-769

Madsen KL, Beuming T, Niv MY, Chang CW, Dev KK, Weinstein H, Gether U (2005) Molecular determinants for the complex binding specificity of the PDZ domain in PICK1. *J Biol Chem* 280: 20539-20548

Marcotte DJ, Hus JC, Banos CC, Wildes C, Arduini R, Bergeron C, Hession CA, Baker DP, Lin E, Guckian KM *et al* (2018) Lock and chop: A novel method for the generation of a PICK1 PDZ domain and piperidine-based inhibitor co-crystal structure. *Protein Sci* 27: 672-680

Menacho-Melgar R, Decker JS, Hennigan JN, Lynch MD (2019) A review of lipidation in the development of advanced protein and peptide therapeutics. *J Control Release* 295: 1-12

Mills SEE, Nicolson KP, Smith BH (2019) Chronic pain: a review of its epidemiology and associated factors in population-based studies. *Br J Anaesth* 123: e273-e283

Missirlis D, Khant H, Tirrell M (2009) Mechanisms of peptide amphiphile internalization by SJSA-1 cells in vitro. *Biochemistry* 48: 3304-3314

Nagy GG, Al-Ayyan M, Andrew D, Fukaya M, Watanabe M, Todd AJ (2004) Widespread expression of the AMPA receptor GluR2 subunit at glutamatergic synapses in the rat spinal cord and phosphorylation of GluR1 in response to noxious stimulation revealed with an antigen-unmasking method. *J Neurosci* 24: 5766-5777

Nishimune A, Isaac JT, Molnar E, Noel J, Nash SR, Tagaya M, Collingridge GL, Nakanishi S, Henley JM (1998) NSF binding to GluR2 regulates synaptic transmission. *Neuron* 21: 87-97

Nissen KB, Andersen JJ, Haugaard-Kedstrom LM, Bach A, Stromgaard K (2015) Design, synthesis, and characterization of fatty acid derivatives of a dimeric peptide-based postsynaptic density-95 (PSD-95) inhibitor. *J Med Chem* 58: 1575-1580

Park JS, Voitenko N, Petralia RS, Guan X, Xu JT, Steinberg JP, Takamiya K, Sotnik A, Kopach O, Huganir RL *et al* (2009) Persistent inflammation induces GluR2 internalization via NMDA receptor-triggered PKC activation in dorsal horn neurons. *The Journal of neuroscience : the official journal of the Society for Neuroscience* 29: 3206-3219

Pastalkova E, Serrano P, Pinkhasova D, Wallace E, Fenton AA, Sacktor TC (2006) Storage of spatial information by the maintenance mechanism of LTP. *Science* 313: 1141-1144

Pedersen MCA, L.; Mortensen, K. (2013) WillItFit: A framework for fitting of constrained models to small-angle scattering data. *J Appl Cryst* 46: 1894-1898

Reinecke H, Weber C, Lange K, Simon M, Stein C, Sorgatz H (2015) Analgesic efficacy of opioids in chronic pain: recent meta-analyses. *Br J Pharmacol* 172: 324-333

Runegaard AH, Jensen KL, Dencker D, Wortwein G, Gether U (2017) Subjective perception of cocaine reward in mice assessed by a single exposure place preference (sePP) paradigm. *J Neurosci Methods* 289: 85-92

Runegaard AH, Jensen KL, Wortwein G, Gether U (2019) Initial rewarding effects of cocaine and amphetamine assessed in a day using the single-exposure place preference protocol. *Eur J Neurosci* 50: 2156-2163

Smith RV, Havens JR, Walsh SL (2016) Gabapentin misuse, abuse and diversion: a systematic review. *Addiction* 111: 1160-1174

Sorensen AT, Rombach J, Gether U, Madsen KL (2022) The Scaffold Protein PICK1 as a Target in Chronic Pain. *Cells* 11

Tan LL, Kuner R (2021) Neocortical circuits in pain and pain relief. *Nat Rev Neurosci*

Tanford C (1972) Micelle shape and size. *J Phys Chem* 76: 3020-3024

Thorsen TS, Madsen KL, Rebola N, Rathje M, Anggono V, Bach A, Moreira IS, Stuhr-Hansen N, Dyhring T, Peters D *et al* (2010) Identification of a small-molecule inhibitor of the PICK1 PDZ domain that inhibits hippocampal LTP and LTD. *Proceedings of the National Academy of Sciences of the United States of America* 107: 413-418

Volk L, Kim CH, Takamiya K, Yu Y, Huganir RL (2010) Developmental regulation of protein interacting with C kinase 1 (PICK1) function in hippocampal synaptic plasticity and learning. *Proceedings of the National Academy of Sciences of the United States of America* 107: 21784-21789

Waldeck W, Pipkorn R, Korn B, Mueller G, Schick M, Toth K, Wiessler M, Didinger B, Braun K (2009) Transporter molecules influence the gene expression in HeLa cells. *Int J Med Sci* 6: 18-27

Wang W, Petralia RS, Takamiya K, Xia J, Li YQ, Huganir RL, Tao YX, Yaster M (2011) Preserved acute pain and impaired neuropathic pain in mice lacking protein interacting with C Kinase 1. *Mol Pain* 7: 11

Wang Z, Yuan Y, Xie K, Tang X, Zhang L, Ao J, Li N, Zhang Y, Guo S, Wang G (2016) PICK1 Regulates the Expression and Trafficking of AMPA Receptors in Remifentanil-Induced Hyperalgesia. *Anesth Analg* 123: 771-781

WHO, 2021. ICD-11 for Mortality and Morbidity Statistics (Version : 05/2021). p. 11th revision.

Wilkerson JL, Curry ZA, Kinlow PD, Mason BL, Hsu KL, van der Stelt M, Cravatt BF, Lichtman AH (2018) Evaluation of different drug classes on transient sciatic nerve injury-depressed marble burying in mice. *Pain* 159: 1155-1165

Woolf CJ, Salter MW (2000) Neuronal plasticity: increasing the gain in pain. *Science* 288: 1765-1769

Xu J, Xia J (2006) Structure and function of PICK1. *Neurosignals* 15: 190-201

Xu Q, Yaksh TL (2011) A brief comparison of the pathophysiology of inflammatory versus neuropathic pain. *Curr Opin Anaesthesiol* 24: 400-407

1 **FIGURES**

2 **Figure 1**

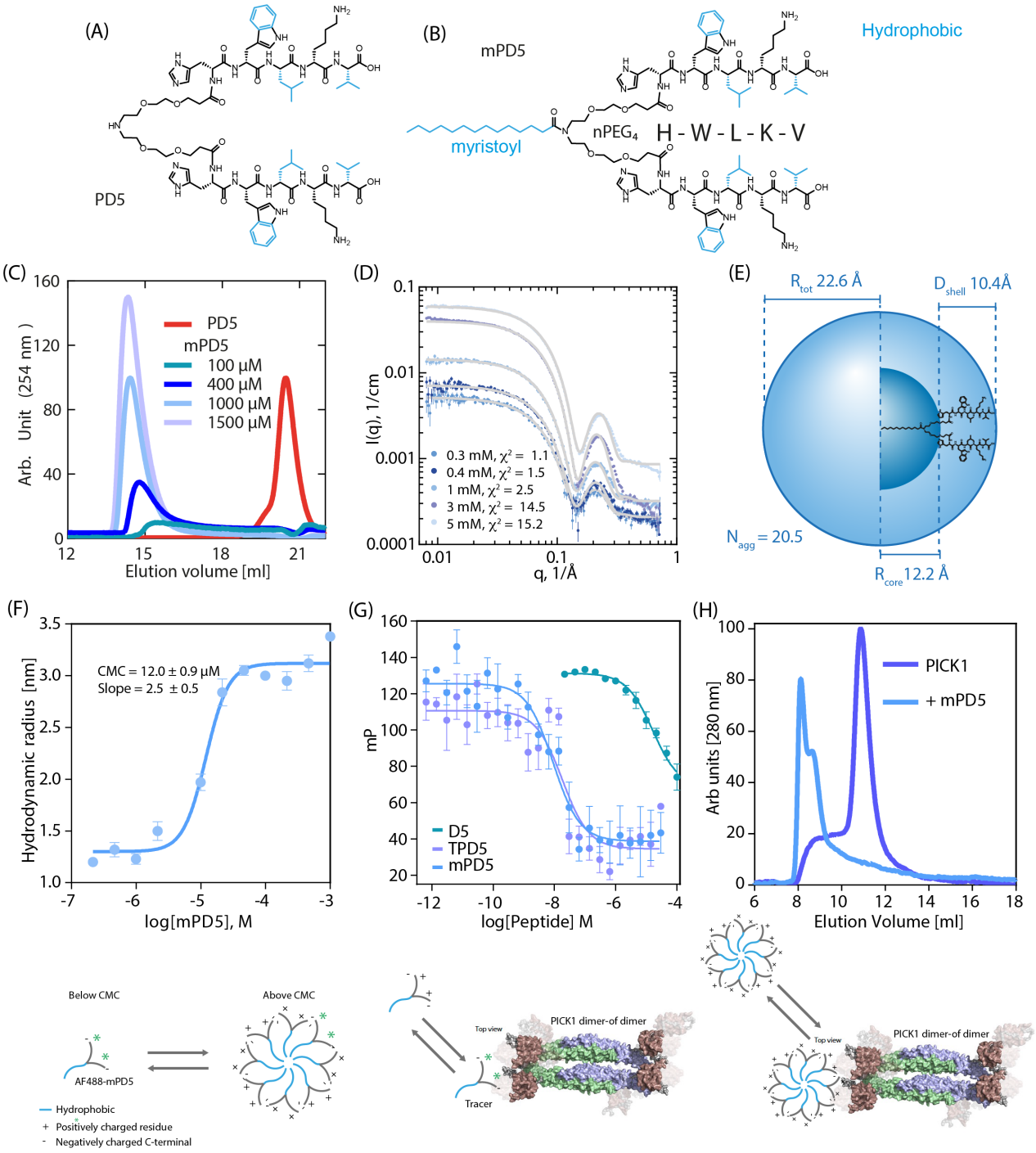

3

4

1 **Figure 2**

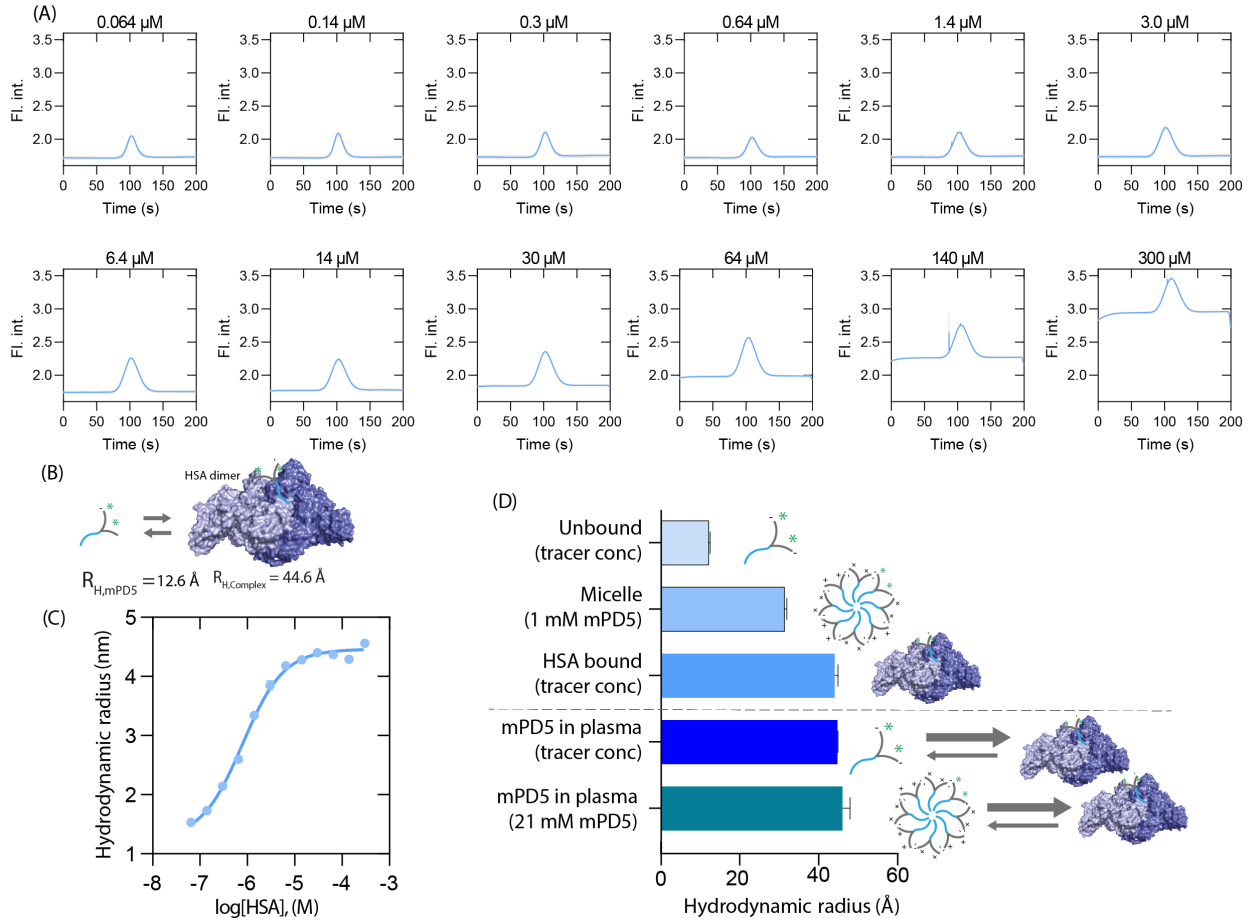
(A)
0.064 µM
0.14 µM
0.3 µM
0.64 µM
1.4 µM
3.0 µM
6.4 µM
14 µM
30 µM
64 µM
140 µM
300 µM
Fl. int.
Time (s)
(B)
HSA dimer
$R_{H,mPD5}$ = 12.6 Å $R_{H,Complex}$ = 44.6 Å
(C)
Hydrodynamic radius (nm)
log[HSA], (M)
(D)
Unbound
(tracer conc)
Micelle
(1 mM mPD5)
HSA bound
(tracer conc)
mPD5 in plasma
(tracer conc)
mPD5 in plasma
(21 mM mPD5)
Hydrodynamic radius (Å)

2

3

1 **Figure 3**

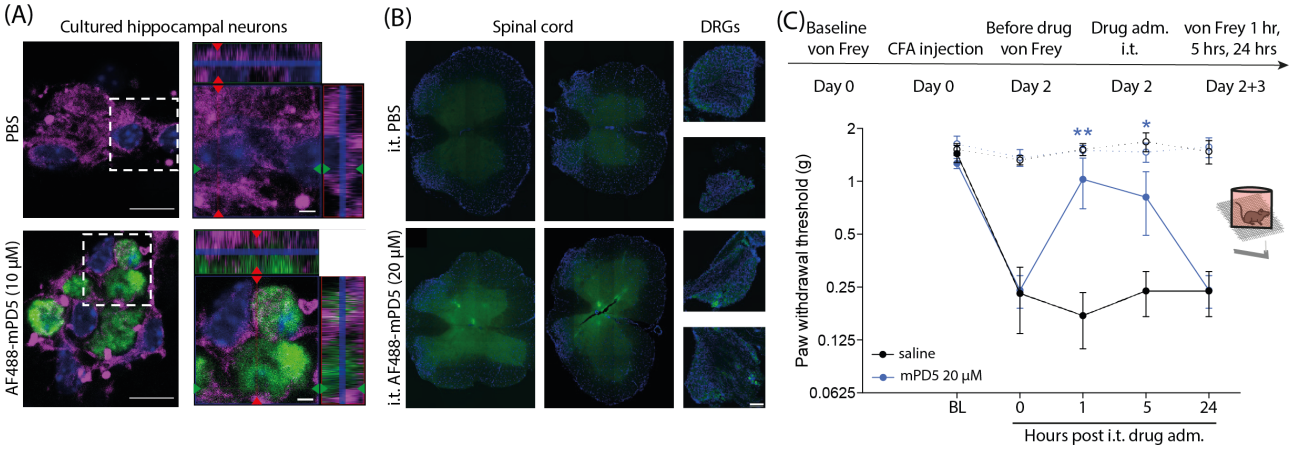
(A)
Cultured hippocampal neurons
PBS
AF488-mPD5 (10 µM)
(B)
Spinal cord
DRGs
i.t. PBS
i.t. AF488-mPD5 (20 µM)
(C)
Baseline von Frey
CFA injection
Before drug von Frey
Drug adm. i.t.
von Frey 1 hr, 5 hrs, 24 hrs
Day 0
Day 0
Day 2
Day 2
Day 2+3
Paw withdrawal threshold (g)
2
1
0.5
0.25
0.125
0.0625
**
*
saline
mPD5 20 µM
BL
0
1
5
24
Hours post i.t. drug adm.

2

3

1 **Figure 4**

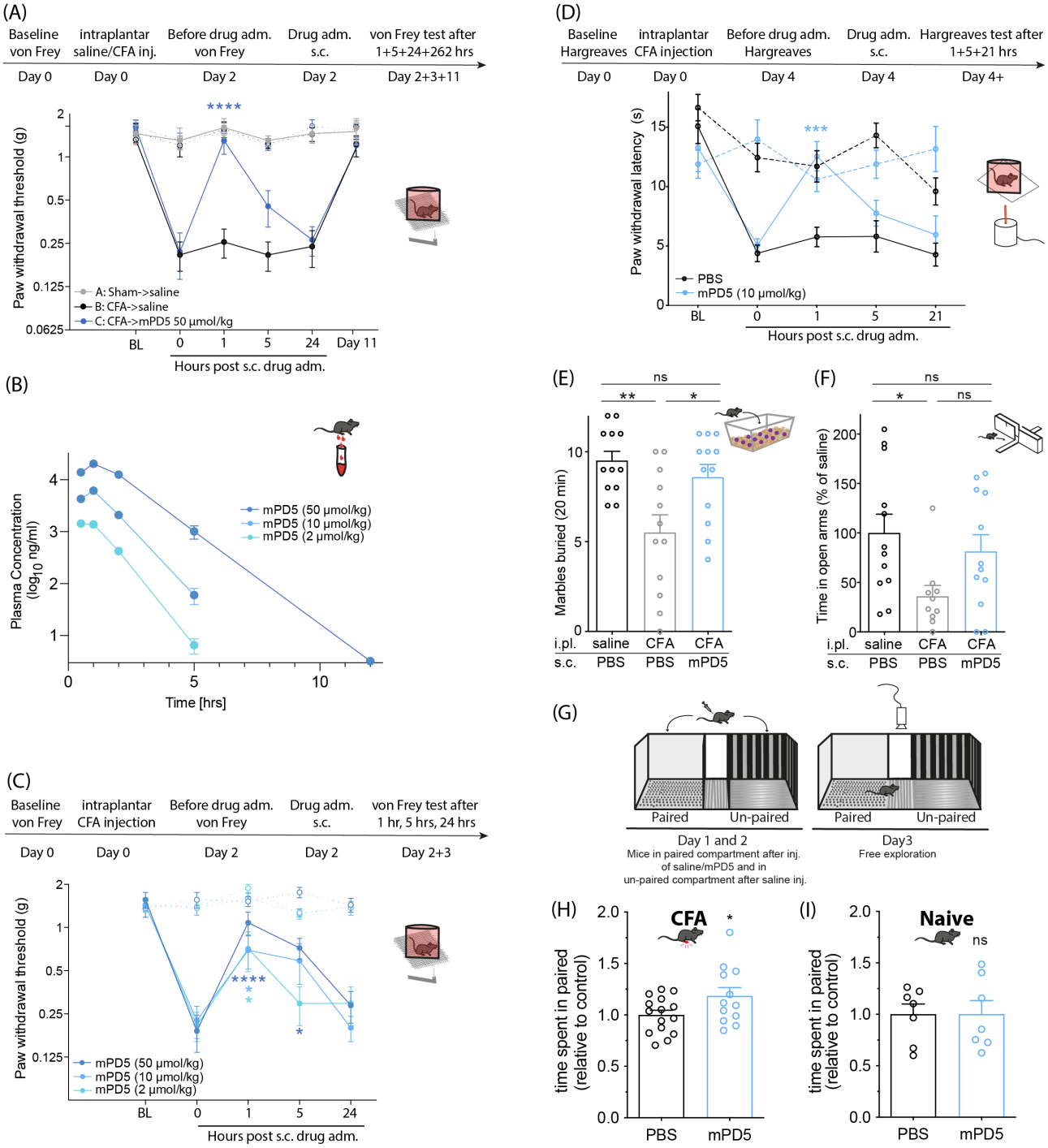

2

3

4

5

6

1 **Figure 5**

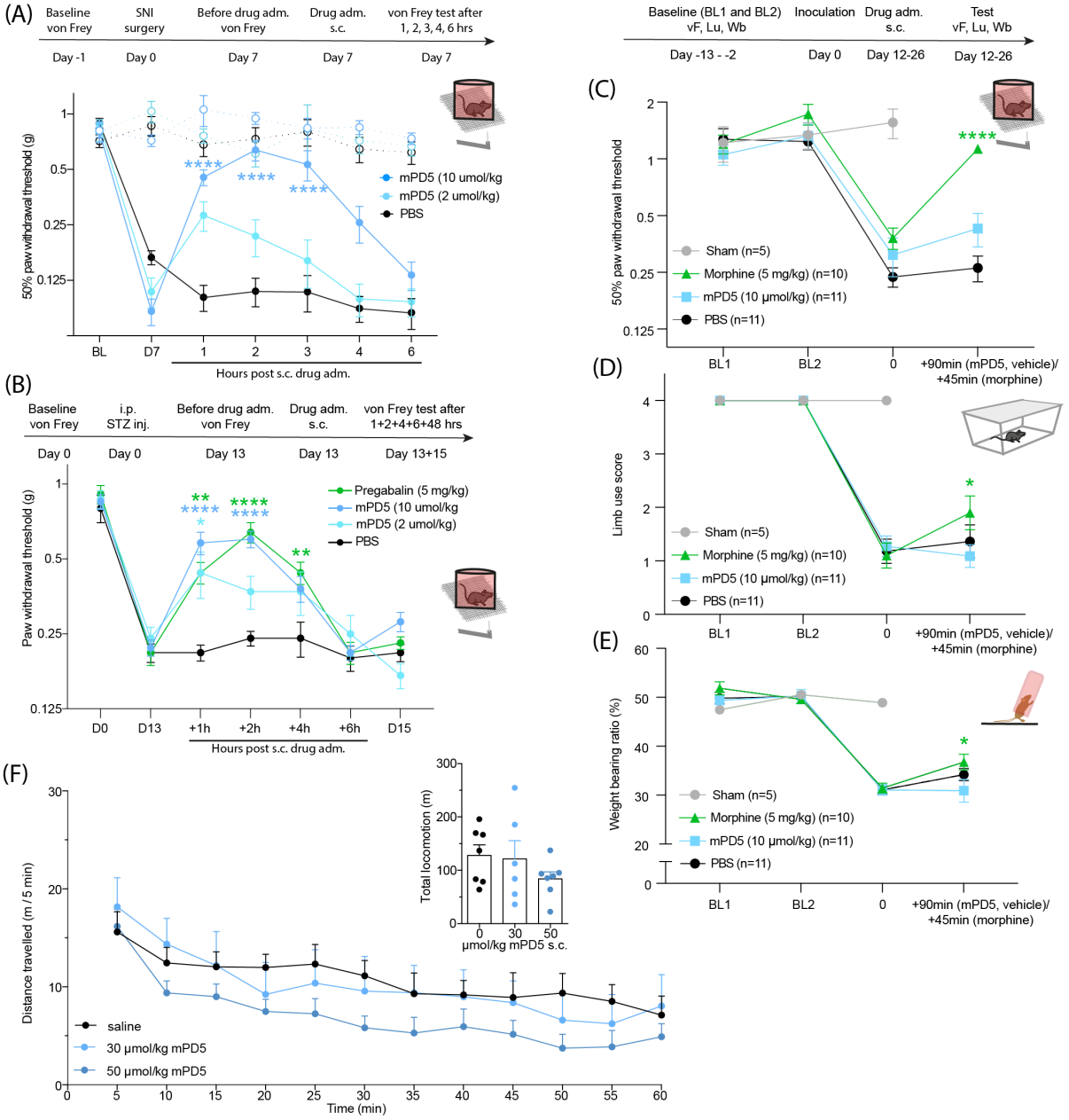

2

3

4

5

6

7

8

1 **Figure 6**

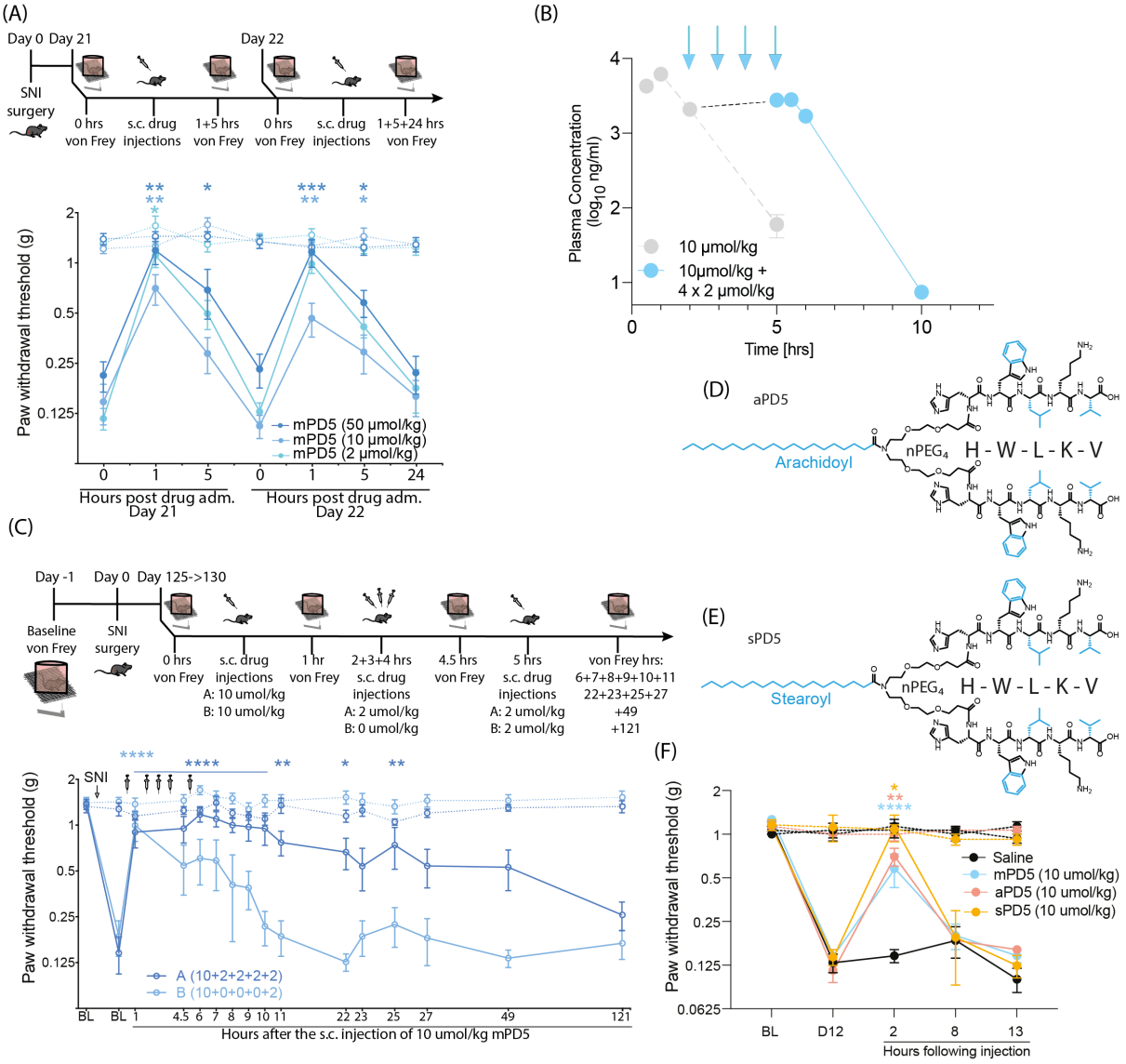
(A)
Day 0 Day 21
Day 22
SNI surgery
0 hrs von Frey
s.c. drug injections
1+5 hrs von Frey
0 hrs von Frey
s.c. drug injections
1+5+24 hrs von Frey
Paw withdrawal threshold (g)
mPD5 (50 µmol/kg)
mPD5 (10 µmol/kg)
mPD5 (2 µmol/kg)
Hours post drug adm. Day 21
Hours post drug adm. Day 22
(B)
Plasma Concentration (log_{10} ng/ml)
10 µmol/kg
10µmol/kg + 4 x 2 µmol/kg
Time [hrs]
(C)
Day -1
Day 0
Day 125->130
Baseline von Frey
SNI surgery
0 hrs von Frey
s.c. drug injections A: 10 umol/kg B: 10 umol/kg
1 hr von Frey
2+3+4 hrs s.c. drug injections A: 2 umol/kg B: 0 umol/kg
4.5 hrs von Frey
5 hrs s.c. drug injections A: 2 umol/kg B: 2 umol/kg
von Frey hrs: 6+7+8+9+10+11 22+23+25+27 +49 +121
SNI
A (10+2+2+2+2)
B (10+0+0+0+2)
Hours after the s.c. injection of 10 umol/kg mPD5
(D)
aPD5
Arachidoyl
nPEG4
H - W - L - K - V
(E)
sPD5
Stearoyl
(F)
Saline
mPD5 (10 umol/kg)
aPD5 (10 umol/kg)
sPD5 (10 umol/kg)
Hours following injection

2

1 ***Table 1*** **Assessment of mPD5 stability.**

	Nominel Conc. mPD5 (μM)	pH	UV-HPLC Peak area	Measured Conc. mPD5 (μM)
30 days 5 °C	200	7.37	6665	194
	50	7.39	3347	49
	20	7.40	1196	17
	2	7.37	37	0.5
	0		ND	<0.2
30 days 25 °C	200	7.36	7005	203
	50	7.41	3325	48
	20	7.39	1161	17
	2	7.37	26	0.4
	0		ND	<0.2

2

FIGURE LEGENDS

Figure 1. Biophysical characterization of mPD5.

Size exclusion chromatography and small angle X-ray scattering demonstrate micellar self-assembly of mPD5. Structure of $NPEG_4$-$(HWLKV)_2$ (PD5) **(A)** and myristoyl-$NPEG_4$-$(HWLKV)_2$ (mPD5) **(B)**, with hydrophobic parts shown in blue. **(C)** Size exclusion chromatography of different concentrations of mPD5 demonstrating self-assembly. **(D)** Small angle X-ray scattering data (points) of mPD5 at different concentrations suggests self-assembly of mPD5 into micelle structures. This is confirmed by the model fits of the core-shell model (overlaying full lines, see supplementary table 1 for fitting parameters). **(E)** Molecular constrained spherical core-shell model fitted to the data (see Fig S1B) suggesting an average of 20.5 molecules per micelle and an average total radius, R_{total} = 22.6 Å. **(F)** Flow-induced dispersion analysis (FIDA) binding isotherm of mPD5 combining optimal coatings for different concentrations (See supplementary Figure S2) results in a CMC of 12 µM and a hydrodynamic radius, R_H of ~ 30 Å. Investigated process illustrated below data. **(G)** Fluorescence polarization (FP) competition binding curves of mPD5 (blue) ($K_{i,app}$ = 3.0 nM, SEM interval [2.3-3.8] nM, n = 6), TPD5 (purple) ($K_{i,app}$ = 3.9 nM, SEM interval [3.5-4.4] nM, n = 3) and D5 (HWLKV) (green) ($K_{i,app}$ = 6998 nM, SEM interval [4972-9849] nM, n = 3), using 5FAM-PD5 (5nM vs.TPD5 and mPD5) or 5FAM-D5 (20 nM vs, D5) as tracer (Error bars are shown as SEM). Data was fitted to a competitive binding One Site fit using GraphPad prism 8.3. Investigated process illustrated below data. **(H)** SEC elution profile of PICK1 in absence (purple) or presence (blue) of mPD5, in a PICK1:mPD5 molecular ratio of 4:1. Investigated process illustrated below data.

Figure 2. mPD5 binds strongly to serum proteins in complex samples matrices.

(A) Taylorgrams from Flow-induced dispersion analysis (FIDA) for different concentrations of HSA and a fixed concentration of AF488-mPD5 (100 nM) using an HS-uncoated capillary. FIDA reveals

widening of taylorgrams as a function of HSA concentration as well as an increased background signal from increased amounts of HSA. **(B)** Binding isotherm of AF488-mPD5 binding to HSA show an affinity (K_D) of 787 nM and a hydrodynamic radius (R_H) of the complex of 4.46 nm. **(C)** The maximal hydrodynamic radius suggests that AF488-mPD5 binds to dimeric HSA. **(D)** Histogram showing the R_H's with SEM obtained for the different experimental conditions of mPD5, suggesting that mPD5 binds to dimeric HSA in plasma rather than forming micelles in plasma, even in the case of excess (21 mM) mPD5. Data was plotted using GraphPad Prism 8.3, and raw data was fitted using FIDA Software (2.0) and resulting hydrodynamic radii was plotted and fitted using a four parameters saturation binding curve with variable slope. Data is expressed as mean ±SEM with n = 3.

Figure 3. Assessment of distribution and analgesic effects of mPD5 in mice following intrathecal administration. (A) Representative confocal images of mouse hippocampal primary cultures incubated without (top panel) or with (bottom panel) AF488-mPD5 (10 µM) (green). Plasma membrane was labelled with CellMask Deep Red (purple) and nuclei with DAPI (blue). Zoomed images (right panel, (extracted from left panel, dashed square)) are maximal projections with orthogonal views at cross-sections indicated by red and green arrows, respectively. Scale bar 10 µm on full pictures (left panel) and 2 µm on the zooms (right panel). **(B)** Representative confocal images of lumbar spinal cord and DRGs slices (L4) from mice injected i.t. with PBS (top panel) or AF488-mPD5 (bottom panel) (20 µM) (green). Nuclei were labelled with DAPI (blue). Scale bar 20 µm. **(C)** Paw withdrawal threshold before and after induction of inflammatory pain (CFA model) and intrathecal (i.t.) treatment with mPD5 or saline. *$P < 0.05$, **$P < 0.01$. Two-way ANOVA followed by Dunnetts *post-hoc* test of time 0 hrs versus 1, 5, 24 hrs. n_{saline}= 5, n_{mPD5} = 6. Abbreviations; adm = administration, CFA = Complete Freund's Adjuvant, i.t. = intrathecal. Data is expressed as mean ±SEM.

Figure 4. Subcutaneous mPD5 provides relief on mechanical and thermal hypersensitivity as well as pain-induced behaviours in a mouse model of inflammatory pain.

(A) Paw withdrawal threshold before and after induction of inflammatory pain (i.p. CFA injection) or sham (i.p. saline injection) and subcutaneous (s.c.) treatment with mPD5 or saline. ****$P < 0.0001$. Two-way ANOVA followed by Dunnetts *post-hoc* test of time 0 hrs versus 1, 5, 24 hrs. n_{saline_saline} = 4, n_{CFA_saline} = 5, n_{CFA_mPD5} = 6. Dashed line = contralateral paw. (**B**) mPD5 was administered s.c. in mice at a 5-fold descending dose range of 2, 10 or 50 µmol/kg. Plasma exposure was determined by LC-MS/MS at 0.5, 1, 2, 5 and 12 hrs following injection. The plasma concentration of mPD5 peaks at 1h post injection in a dose-dependent manner ((1.4 ± 0.1 mg/mL after 2 µmol/kg injection; 6.2 ± 5 mg/mL after 10 µmol/kg injection; 20.2 ± 0.6 mg/mL after 50 µmol/kg injection)). mPD5 is eliminated with linear kinetics. **(C)** Paw withdrawal threshold before and after induction of inflammatory pain (CFA model) and subcutaneous (s.c.) treatment with mPD5. *$P < 0.05$, ****$P < 0.0001$. Two-way ANOVA followed by Dunnetts *post-hoc* test of time 0 hrs versus 1, 5, 24 hrs. n_{50} = 5, n_{10} = 6, n_2 =5. Dashed line = contralateral paw. **(D)** Paw withdrawal latency before and after induction of inflammatory pain (CFA model) and subcutaneous (s.c.) treatment with mPD5 or PBS. ***$P < 0.001$. Two-way ANOVA followed by Dunnetts *post-hoc* test of time 0 hrs versus 1, 5, 21 hrs. n= 6 in both groups. Dashed line = contralateral paw. **(E)** Marbles buried by mice 3 days after induction of inflammatory pain (i.p. CFA injection) or sham (i.p. saline injection) and 1 hour post subcutaneous (s.c.) treatment with mPD5 or PBS. *$P < 0.05$, **$P < 0.01$. one-way ANOVA with Tukey multiple comparison. n = 12 in each group. **(F)** Time spent in open arms of an elevated plus maze relative to sham, 2 days after induction of inflammatory pain (i.p. CFA injection) or sham (i.p. saline injection) and 1 hour post subcutaneous (s.c.) treatment with mPD5 or PBS. *$P < 0.05$, **$P < 0.01$. one-way ANOVA with Tukey multiple comparison. n = 12 in each group. **(G)** schematic

overview of single-exposure place preference (sePP) test with to counter-balanced days of conditioning followed by a test day. **(H)** Time spent in the paired compartment of CFA mice treated with 30 µmol/kg (10 µL/gram) mPD5 or saline in the paired compartment. *$P < 0.05$. unpaired t-test. n_{PBS}= 13, n_{mPD5} = 12. **(I)** Time spent in the paired compartment of Naïve mice treated with 30 µmol/kg (10 µL/gram) mPD5 or saline in the paired compartment. unpaired t-test. n = 7 in both groups.

Abbreviations; adm. = administration, BL = baseline, CFA = Complete Freund's Adjuvant, hrs = hours, inj. = injection, i.pl. = intraplantar, i.t. = intrathecal, s.c. = subcutaneous, sePP = single exposure place preference. All data is expressed as mean ±SEM.

Figure 5. Subcutaneous mPD5 reduces mechanical hypersensitivity of neuropathic pain and diabetic neuropathy but not bone cancer induced pain. (A) Paw withdrawal threshold before and after induction of neuropathic pain (SNI surgery) and subcutaneous (s.c.) treatment with mPD5 or PBS 7 days after surgery. ****$P < 0.0001$. Two-way ANOVA followed by Dunnetts *post-hoc* test of time 0 hrs versus 1, 2, 3, 4 and 6 hrs. n = 6 in each group. Dashed line = contralateral paw. **(B)** Paw withdrawal threshold before and after induction of diabetic neuropathy (STZ injection) and subcutaneous (s.c.) treatment with mPD5, Pregabalin or PBS 13 days after STZ injection. *$P < 0.05$, **$P < 0.01$, ****$P < 0.0001$. Two-way ANOVA followed by Dunnetts *post-hoc* test of time 0 hrs versus 1, 2, 4, 6 and 24 hrs. $n_{pregabalin}$ = 10, n_{mPD5} = 10 and n_{PBS} = 9. **(C-E)** Efficacy of mPD5 in mice with cancer induced bone pain or sham animals. $n_{morphine}$ = 10, n_{mPD5} = 11 and n_{PBS} = 11. **(C)** Paw withdrawal threshold before and after induction of cancer induced bone pain (sham or NCTC 2472 cell inoculation) and subcutaneous (s.c.) treatment with mPD5, morphine or PBS. ****$P < 0.0001$. Two-way ANOVA followed by Dunnetts *post-hoc* test of pre versus post + baselines. **(D)** As in panel C, but for limb use score *$P < 0.05$. Wilcoxon matched-pairs signed rank test (non-parametric data).

(E) As in panel C, but for weight bearing. *$P < 0.05$. Two-way ANOVA followed by Dunnetts *post-hoc* test of pre versus post and baselines**. (F)** One hr open field test of naïve mice 60 min after subcutaneous (s.c.) injection of saline or mPD5 with distance travelled in (5 min bins) and total distance (insert). Two-way ANOVA followed by Dunnetts *post-hoc* analysis). $n_{saline} = 7$, $n_{30} = 6$, $n_{50} = 7$.

All data is expressed as mean ±SEM. Abbreviations; adm. = administration, BL = baseline, D = day, hrs = hours, inj. = injection, i.p. = intraperitoneal, i.pl. = intraplantar, Lu = limb use score, s.c. = subcutaneous, stz = streptozocin, SNI = spared nerve injury, Wb =weight bearing ratio.

Figure 6. mPD5 provides extended relieve of mechanical hypersensitivity in a model of late-stage neuropathic pain following sustained dosing. (A) Paw withdrawal threshold before and after induction of neuropathic pain (SNI surgery) and repeated subcutaneous (s.c.) treatment with mPD5 22 days after surgery. *$P < 0.05$, **$P < 0.01$, ***$P < 0.001$. Two-way ANOVA followed by Dunnetts *post-hoc* test of time 0 hrs versus 1, 5 and 23, 24, 29 and 48 hrs after first injection. 2way ANOVA, dunnetts post-test, compared to baseline post SNI. n = 8 in each group. **(B)** Plasma concentration of mPD5 (blue) determined by LC-MS/MS in mice injected s.c. with 10 µmol/kg mPD5 followed by 2+2+2+2 µmol/kg mPD5 once an hr. mPD5 was eliminated with linear kinetics similar to the single administration (Gray, dashed line, identical to Figure 4B), shown again for comparison. **(C)** Paw withdrawal threshold before and after induction of neuropathic pain (SNI surgery) and sustained subcutaneous (s.c.) treatment with 10 + 2 + 2+ 2 + 2 µmol/kg or 10 + 0 + 0 + 0 + 2 µmol/kg (one hr between injections) mPD5, 125 days (18 weeks) after surgery. *$P < 0.05$, **$P < 0.01$, ****$P < 0.0001$. Two-way ANOVA followed by Dunnetts *post-hoc* test vs baseline before treatment. n=8 in each group. **(D)** Structure of arachidoyl-NPEG$_4$-(HWLKV)$_2$ (peptide conjugated with C20 (arachidic acid)) (aPD5) and **(E)** Stearoyl-NPEG$_4$-(HWLKV)$_2$ (peptide conjugated with C18 (stearic acid))

(sPD5) **(F)** Paw withdrawal threshold before and after induction of neuropathic pain (SNI surgery) and subcutaneous (s.c.) treatment with saline, aPD5, sPD5 or mPD5 12 days after surgery. *$P < 0.05$, **$P < 0.01$, ****$P < 0.0001$. Two-way ANOVA followed by Dunnetts *post-hoc* test of time 0 hrs versus 2, 8 and 13 hrs. n = 6 in each group. Dashed line = contralateral paw.

All data is expressed as mean ±SEM. Abbreviations; adm. = administration, BL = baseline, D = day, hrs = hours, inj. = injection, s.c. = subcutaneous, SNI = spared nerve injury. The dashed line is data on the contralateral paw.